International Journal of Nanomedicine

Dovepress
Taylor & Francis Group

Open Access Full Text Article

REVIEW

The Advanced Application of Halide Perovskite Materials for Gas Sensor

Yue Li[1,*], Zhiwen Qiu[2,*], Jinwei L Lai[3], Qilin Xu[3], Yue Wu[3], Can Jiang[3], Bingbing Li[2], Yueyue Li[2], Wei Li[1,2]

[1]School of Health Science and Engineering, University of Shanghai for Science and Technology, Shanghai, 200093, People's Republic of China; [2]Department of Nanomedicine, Shanghai Key Laboratory of Nautical Medicine and Translation of Drugs and Medical Devices, Naval Medical University, Shanghai, 200433, People's Republic of China; [3]School of Gongli Hospital Medical Technology, Oriental Pan-Vascular Devices Innovation College, University of Shanghai for Science and Technology, Shanghai, 200093, People's Republic of China

*These authors contributed equally to this work

Correspondence: Wei Li, Email liwei_dds@163.com

Abstract: The demand for highly functional chemical gas sensors has surged in response to critical needs such as health monitoring, protection against harmful gases, and assessment of food freshness. Over the past few decades, various chemiresistive gas sensors have been developed, exhibiting considerable sensitivity to a range of gases. However, their performance remains constrained by notable drawbacks, including elevated operating temperatures, inadequate sensitivity, and poor selectivity. In recent years, perovskite materials have garnered substantial attention due to their exceptional chemical and physical properties-such as a high absorption coefficient, low ionic binding energy, tunable bandgap, and high carrier mobility. Concurrently, significant strides have been made in leveraging both organic and inorganic perovskite-based sensors for detecting environmental gases. This review provides a comprehensive overview of the recent advancements in perovskite-based gas sensors, systematically analyzing the field from material design and engineering to device applications. We dissect the critical influence of perovskite crystal structures and micro/nano-architectures on key performance metrics such as sensitivity, selectivity, response/recovery time, and stability. The applications of these materials in detecting a wide array of hazardous gases—including H_2S, NH_3, NOx, CO/CO_2, and various volatile organic compounds (VOCs)—are thoroughly examined, with representative examples and underlying sensing mechanisms discussed in detail. However, the path to commercialization is obstructed by persistent challenges of instability, selectivity, and the severe environmental and health risks of lead. This has catalyzed a major research thrust towards non-toxic, lead-free perovskites. Consequently, the field is pivoting towards lead-free perovskites. This analysis underscores that synergistic innovation in lead-free material science and device engineering is critical to overcoming current barriers, paving the way for the development of robust, high-performance, and commercially viable gas sensors that align with global sustainability goals.

Keywords: perovskite, mechanisms, gas sensor

Introduction

With the rapid advancement of science and technology, people's quality of life has been significantly enhanced. However, air pollution remains an unavoidable issue. Toxic and harmful gases emitted from industrial sources are a primary contributor to air pollution, posing severe threats to human health and even inflicting irreparable damage on the global environment. According to statistics from the World Health Organization (WHO),[1] Approximately 7 million deaths each year are attributed to respiratory illnesses-including bronchitis, pneumonia, and lung cancer-linked to air pollution.[2] Meanwhile, the escalating demands across multiple fields-including real-time industrial safety monitoring, medical gas biomarker screening, precise indoor air quality control, and non-destructive food freshness detection-have imposed stringent requirements on gas sensors: ultra-trace detection, high selectivity with anti-interference capability, real-time response, and low-cost scalability.[3] Currently, a wide range of gas sensors are available, which can be classified into different categories based on their sensing mechanisms[4] These include thermal conductivity sensors, semiconductor

Received: 21 July 2025
Accepted: 28 November 2025
Published: 21 December 2025

Graphical Abstract

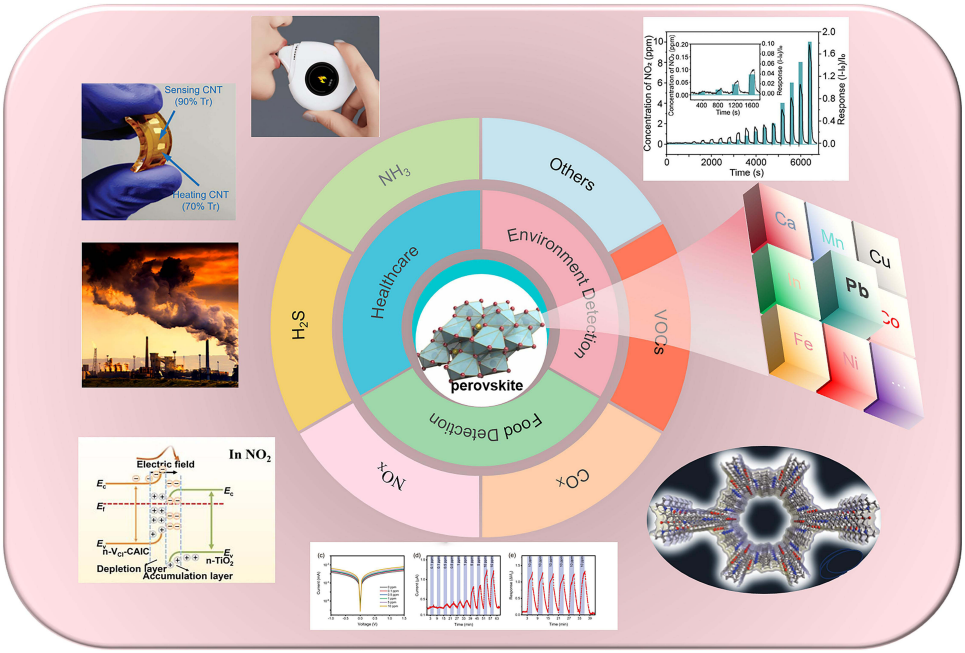

metal oxide (SMO) sensors, infrared absorption sensors, catalytic combustion sensors, electrochemical sensors, and solid electrolyte sensors. Alternatively, they can be categorized according to their interaction principles with target gases, such as photoelectric sensors, all-optical conversion sensors, electrocatalytic sensors, physicochemical loading sensors, and surface plasmon resonance (SPR) sensors.[5]

Prior to 2019, materials such as graphene, semiconductor metal oxides, carbon, and black phosphorus were widely utilized in gas sensors. These materials gained favor due to their simple structure, low cost, and rapid response. Despite these advantages, their widespread commercial adoption was hindered by inherent limitations, including poor sensitivity, inadequate selectivity, and a reliance on high operating temperatures. This thermal requirement posed a significant challenge, escalating both energy consumption and fabrication costs through the integration of heating elements. Moreover, prolonged exposure to high temperatures degraded the long-term stability and repeatability of the sensors by causing detrimental changes in the nanostructure's phase, morphology, or composition. In recent years, perovskite has drawn considerable attention, thanks to its exceptional chemical and physical properties-such as a high absorption coefficient, low ionic binding energy, tunable bandgap, and high carrier mobility, low work temperature. Moreover, the photoelectric conversion electrical signals, absorption spectra, and all-optical conversion luminescence spectra of perovskite materials can be adjusted. This tunability allows for the optimization of their responses to different gases, thereby enhancing detection sensitivity.[6] Furthermore, perovskite materials offer advantages such as low synthesis costs, simple preparation processes, relatively low operational requirements, and ease of use. Their versatility in morphology is particularly notable; for instance, halide perovskite quantum dots (HaPs QDs) exhibit high surface activity, enabling rapid adsorption and desorption of gas molecules, which enhances real-time performance and detection accuracy. However, a significant challenge remains: the intrinsic instability of HaPs QDs.[7] Persistent exposure to heat and light can weaken the Pb-X chemical bonds, leading to structural degradation. This critical issue has spurred extensive research into the surface properties of HaPs QDs and their interactions with the environment, aiming to design mechanisms that enhance their stability against light irradiation and polar solvents. To address these concerns, various surface-stabilizing techniques were developed around 2020, such as encapsulation within inorganic matrices, polymer embedding, compositional engineering, and phase transformation. These encapsulation strategies not only shield and stabilize the QDs from

external stimuli but also prevent the leakage of harmful lead ions into the environment. Following these breakthroughs, several studies have successfully demonstrated the fluorescence imaging and biosensing capabilities of HaPs QDs, with $CsPbBr_3$ QDs being particularly favored for their superior stability compared to chloride- and iodide-based counterparts.[8,9] In a significant recent trend, research is shifting towards lead-free halide perovskites to address toxicity concerns without compromising their superior performance. This approach is exemplified by efforts to fabricate durable, non-toxic, and highly stable gas sensors using specific lead-free perovskite nanocrystals (NCs). Crucially, the inherent versatility of perovskites, along with their facile synthesis and integration, positions them as promising candidates for commercial-scale manufacturing.[10]

The core of this review is a detailed examination of the state-of-the-art applications of halide perovskites in detecting a wide spectrum of hazardous gases. For each target gas—including hydrogen sulfide (H_2S), ammonia (NH_3), nitrogen oxides (NOx), carbon oxides (CO/CO_2), and various volatile organic compounds (VOCs)—we summarize representative research progress, highlight key material designs, and dissect the underlying sensing mechanisms. We further explore the fundamental principles governing gas-perovskite interactions, such as surface adsorption and chemical reactions, changes in optical properties, ion migration, and surface plasmon resonance effects. Finally, the review addresses the significant challenges that impede commercialization, such as intrinsic instability, poor reproducibility, and the critical issue of lead toxicity, while also touching upon emerging strategies like the development of lead-free alternatives to mitigate these concerns. This structured overview provides a valuable resource for understanding the current landscape and guiding future research in perovskite-based gas sensing. As shown in Figure 1, the development trends of halide perovskites used in gas sensing research over the past five years are listed.

Perovskite

Crystal Structure

Perovskite solar cells derive their name from the crystal structure of their light-absorbing materials, typically represented by the general formula ABX_3.[21] Originally describing the calcium titanium oxide mineral, the term "perovskite" has been generalized to include any material sharing this distinctive structure, as illustrated in Figure 1. In this framework, the constituent ions define the material's class: an inorganic halide perovskite features an A-site occupied by inorganic cations like Cs+ or K+. Conversely, an organic-inorganic hybrid perovskite incorporates organic cations such as CH_3NH_3 + (MA+) or $(NH_2)_2CH$+ (FA+) at the A-site, which serve to stabilize the structure within the octahedral voids.[22] The

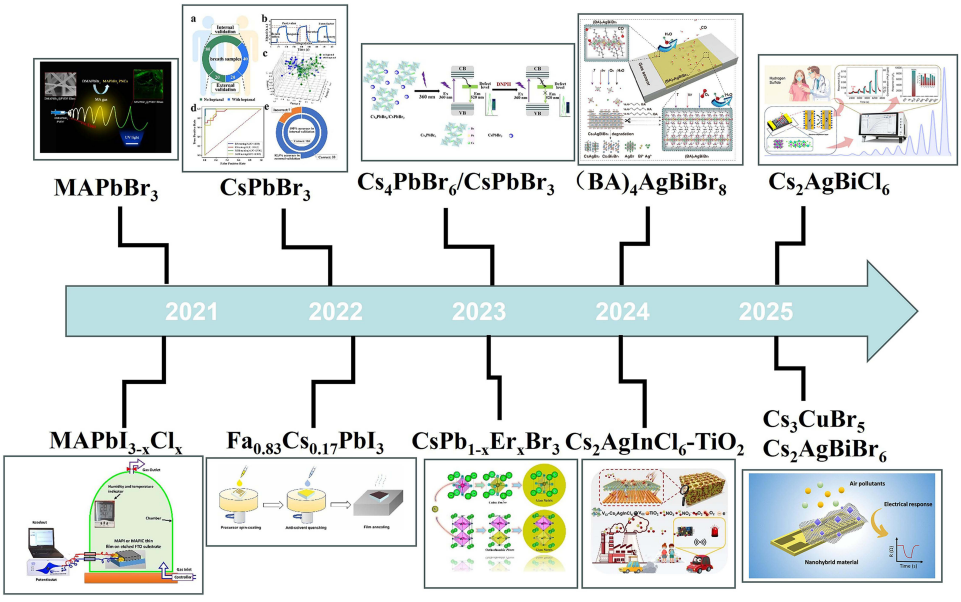

Figure 1 Trend chart of halide perovskites in the past five years.[11–20]

https://doi.org/10.2147/IJN.S554538

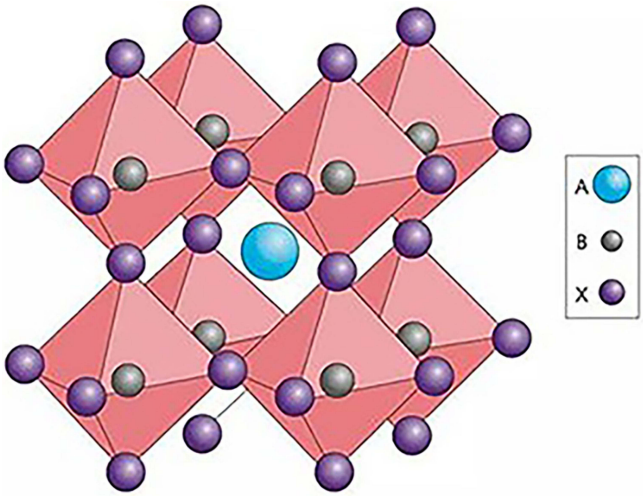

Figure 2 The crystal structure of peroskite.[24]

B-site, located at the center of the octahedron, is typically occupied by divalent cations (eg, Pb^{2+}, Sn^{2+}) or tetravalent cations (eg, Ti^{4+}), while the X-site consists of halide anions (Cl^{-}, Br^{-}, I^{-}). Beyond the standard ABX_3 lattice, related structures like $CsPb_2X_5$, Cs_4PbX_6, and $A_2B(I)B(III)X_6$ also exist, highlighting the vast compositional diversity of the perovskite family.[23] The structure of the perovskite is shown in Figure 2.

For gas sensing applications, perovskite materials can be broadly categorized into three types—inorganic, organic, and organic-inorganic hybrids-each presenting a unique trade-off between stability, tunability, and performance. Inorganic perovskites excel in stability and electron mobility, facilitating long-term operation in harsh industrial environments (eg, high temperature, humidity) and enabling rapid gas responses. Their key limitations are limited chemical tunability and poor gas selectivity. Organic perovskites present the opposite profile: they are inherently unstable under environmental stress, hindering reusability, but their molecular structures are highly modifiable. This allows for the optimization of gas adsorption via functional group engineering, offering a pathway to high theoretical selectivity, albeit primarily for controlled laboratory applications. Organic-inorganic hybrid perovskites represent a strategic compromise, merging the robustness of inorganic components with the chemical flexibility of organic ones. This synergy has established them as the dominant platform in the field. They deliver high response values due to superior optoelectronic activity and offer structural versatility for device integration. While their stability meets the needs of conventional detection (e.g, indoor air monitoring), they still fall short of the extreme-environment tolerance exhibited by purely inorganic perovskites.

Effects of Perovskite Microstructure on Gas Sensing Properties

Perovskites are highly suitable for resistive-type gas sensors, owing to their structural stability derived from abundant metallic elements, tunable composition via aliovalent cation substitution at A/B sites, tolerance to non-stoichiometry, and unique electronic properties characterized by high electron mobility. In perovskites, oxygen vacancies tend to dominate over cationic vacancies due to their lower formation energy. The coexistence of both vacancy types enhances the material's electrical conductivity, redox activity, and catalytic performance-all of which critically influence gas-sensing behavior.

Additionally, their inherent mechanical and thermal stability enables reliable operation across a broad temperature range, further solidifying their suitability for sensing applications. The gas-sensing performance of perovskite materials is highly dependent on their microstructure, necessitating precise control through tailored preparation methods. By employing advanced synthesis techniques and optimizing key parameters, perovskite nanostructures can be engineered to possess enhanced morphological properties, which significantly improve their sensitivity-particularly for the detection of low-concentration gases.[25]

Nanostructured materials boast a high density of active surface sites and efficient gas diffusion pathways, which dramatically enhance interfacial interactions with target gas molecules.[26] In perovskite-based gas sensors, critical micromorphological characteristics-including specific surface area (SSA), porosity, grain size, and grain stacking-directly govern sensing performance. To optimize these parameters, engineered nanostructures such as nanoparticles, nanorods, and nanospheres are strategically employed to maximize gas-sensing efficiency. Additionally, architectures featuring wrinkled surfaces or hierarchical porosity (meso-/macropores) further increase SSA, facilitating enhanced gas adsorption and amplifying electrical signal transduction upon gas exposure. For instance, Xiao et al[27] utilized electrospinning to fabricate $LaFeO_3$ into a hollow nanofiber structure, substantially increasing its specific surface area (SSA). Furthermore, the uniform dispersion of Pt nanoparticles on the $LaFeO_3$ nanofibers enhanced catalytic activity; the optimal response value of Pt-functionalized $LaFeO_3$ is approximately 2.5 times that of pristine $LaFeO_3$. This improvement was attributed to synergistic effects, including increased oxygen vacancies, Pt's catalytic promotion, and the unique hollow morphology. In conclusion, optimizing surface complexity and porosity in perovskite materials significantly enhances gas-sensing performance by improving gas adsorption and charge transfer dynamics. These microstructural advancements provide a robust foundation for developing next-generation gas sensors with exceptional sensitivity and selectivity, paving the way for high-performance nanomaterial-based detectors.

Gas Sensing Performance Parameters

The performance of gas sensors is characterized by several critical parameters that collectively determine their effectiveness. Key evaluation metrics include sensitivity, response/recovery time, selectivity, long-term stability, optimal operating temperature, and detection limit. Each of these parameters plays a vital role in defining the sensor's overall performance characteristics, as elaborated in the following discussion.[28]

Sensitivity

Gas-sensitive responsiveness is a crucial parameter of gas sensors, typically quantified by the rate of change in electrical signals. For n-type semiconductor materials, sensitivity is defined as the ratio of the stable resistance value before exposure to the target gas to that after exposure (Ra/Rg). In contrast, for p-type semiconductor materials, sensitivity is expressed as the inverse ratio (Rg/Ra). Here, Ra denotes the resistance in the absence of the target gas, while Rg refers to the resistance in the presence of the target gas.[28]

Response and Recovery Time

The response time (tres) refers to the duration required from the introduction of the target gas until the resistance value reaches 90% of its stable state. The recovery time (trev) is the time needed from the desorption of the gas until the resistance value returns to 90% of its initial stable value.

Selectivity

Selectivity refers to the ability to exhibit a relatively high response to the target gas while showing minimal response to other gases. It reflects strong specificity and tracking capability for the target gas. The higher the selectivity of the sensor, the stronger its anti-interference performance, making it more advantageous for practical applications.

Stability

Stability refers to the ability of a gas sensor to maintain consistent performance throughout its operational period. Over time, the sensor's gas-sensing characteristics-including sensitivity, selectivity, response time, and recovery time-should remain relatively stable These parameters are commonly used to evaluate the stability of a gas sensor.

Optimal Working Temperature

The optimal operating temperature is the temperature at which the sensitivity of the gas sensor reaches its maximum. The temperature of the sensing material directly influences the sensing performance of chemiresistive gas sensors.

Detection Limit

The detection limit refers to the lowest concentration of the target gas that can be recognized. This parameter plays an important role in fields such as disease diagnosis and the monitoring of toxic and harmful gases. Different application scenarios have varying requirements for the detection limit. A lower detection limit means the sensor can detect the target gas in the environment at an earlier stage, thereby enhancing its sensitivity and practical applicability.

Gas-Sensing Applications of Halide Perovskites

Toxic gases such as ammonia (NH_3), hydrogen sulfide (H_2S), nitrogen oxides (NO_x), carbon oxides (CO, CO_2), and various toxic vapors are prevalent in industrial emissions, environmental pollutants, and daily life scenarios, posing a grave threat to human health and the ecological environment. Halide perovskites show remarkable potential in toxic gas detection due to their unique material properties.[29] This section will systematically analyze these hazardous gases, covering their detection mechanisms, recent research advances, key performance determinants, and practical application scenarios.

Detection of Hydrogen Sulfide

Hydrogen sulfide (H_2S), a colorless and highly toxic gas with a characteristic rotten eggs smell, is frequently present in places such as deep wells, sewers, oil refineries, biogas digesters, and landfills. Its corrosivity towards industrial equipment, coupled with its health risks-irritating the respiratory tract at low concentrations and causing fainting or death at high concentrations-underscores the critical need for real-time H_2S monitoring.[30] In 2022, Ayesh et al[31] synthesized formamidinium lead bromide ($FAPbBr_3$) nanoparticles with an average size of 23 ± 8 nm via a simple solution-growth method. The gas sensor fabricated using these nanoparticles exhibited high sensitivity to H_2S in the range of 0.5–100 ppm with a response time of less than one minute at room temperature. The sensing mechanism is based on a physical change. The adsorption of H_2S gas on the nanoparticles surface alters their surface charge, thereby inducing a change in the material's electrical conductivity. In the same year, Lee et al[32] synthesized $MAPbI_3$ and a pseudohalide anion (SCN^-)-doped perovskite, $MAPbI_{3-x}(SCN)_x$. When the H_2S concentration was 200 ppb, the response rate of the $MAPbI_3$ based sensor was 5.6%, whereas that of the $MAPbI_{3-x}(SCN)_x$ sensor was 14.8%. When the H_2S concentration was 1000 ppb, the response rate of the $MAPbI_3$ sensor was 15.8 ± 1.7%, and that of the $MAPbI_{3-x}(SCN)_x$ sensor was 50.6 ± 4.4%. Furthermore, the service life of $MAPbI_3$ generally does not exceed 24 hours, while that of $MAPbI_{3-x}(SCN)_x$ can be up to 5 days. In addition, the gas-sensing performance was compared under relative humidity (RH) conditions of 24%, 46%, and 64%, and it was found that this sensor can overcome the challenge of high-humidity environments. The interaction between the cation (Pb^2+) and the anion (SCN^-), as well as the hydrogen bond existing between SCN^- and MA+, improve the stability of the material.

Inorganic halide perovskites can also be used for the detection of H_2S gas. In 2023, Zhang et al[33] prepared a composite material $CsBr/Cs_3Bi_2Br_3I_6$ using a two-step evaporation-spraying method. The toxic Pb^2+ was replaced by Bi^3+. The fabricated sensor shows a good response to H_2S. This is because H_2S reacts with the composite material, forming an S-O asymmetric peak, which then triggers the adsorption-desorption process and dynamic defect passivation. At room temperature, the sensor can detect H_2S at a concentration as low as 0.5 ppm, and the device can maintain its stability for more than 60 days. The composite material not only improves the stability but also enhances the detection efficiency, providing a new path for the development of sensors in Figure 3. In the same year, Ou et al[34] prepared a lead-free halide perovskite $CsCu_2I_3$ through a one-step CVD method. A gas sensor was fabricated by depositing a $CsCu_2I_3$ thin film on a glass substrate with pre-fabricated interdigitated ITO electrodes. It can detect H_2S at a concentration as low as 0.2 ppm, with a response value of 0.5, and it exhibits a stability of up to 45 days. The atomic percentage of iodine in $CsCu_2I_3$ is less than 50%, indicating the presence of a large number of iodine vacancies. These vacancies can act as electron traps, enhancing the interaction with the gas. The perovskite $CsCu_2I_3$ shows great potential for applications in H_2S gas detection in Figure 4a. In 2024, Zhang et al[35] prepared chiral quasi-two-dimensional perovskite nanomaterials, $Bio(S\text{-}PEA)_2CsPb_2Br_7$ and $Bio(R\text{-}PEA)_2CsPb_2Br_7$. As probes, they exhibit a rapid and sensitive fluorescence quenching response to H_2S. The chiral perovskites employ surface passivation and polymer encapsulation techniques, which

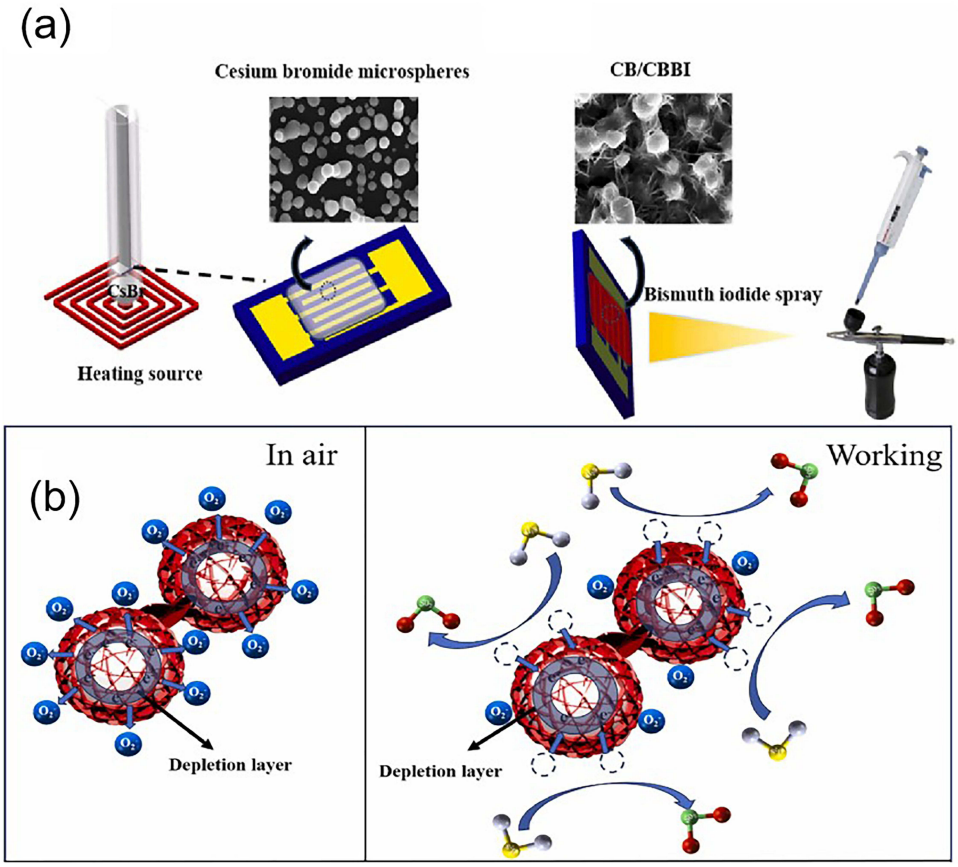

Figure 3 (**a**) Schematic diagram of the synthesis process of $CsBr/Cs_3Bi_2Br_3I_6$. (**b**) Schematic diagram of the gas-sensing mechanism of the $CsBr/Cs_3Bi_2Br_3I_6$ thin film.[33]

significantly improve their stability, enabling them to maintain stability in water for more than 60 days. This not only retains the photoluminescence properties of perovskite materials but also enhances their biocompatibility, laying a foundation for the application of perovskites in life sciences. Subsequently Huang et al[36] synthesized the composite material $CsPbBr_3$-Fe_2O_3, which can be used to detect H_2S at the ppb level. At a high temperature of 350 °C, when the H_2S concentration is 10 ppm, the sensor exhibits a response value of 4.12, with a response time and recovery time are 1.84s and 24.2s respectively. This excellent gas-sensing performance may be attributed to the formation of a heterojunction, which improves the migration efficiency of electrons from $CsPbBr_3$ to Fe_2O_3, resulting in a wider depletion region and enhanced sensor response to H_2S. This material offers a promising strategy for improving the sensitivity and stability of perovskite nanomaterials to harmful gases such as H_2S. In 2025, Casanova-Chafer[11] and others synthesized lead-free perovskites Cs_3CuBr_5 and $Cs_2AgBiBr_6$ supported on graphene. Moreover, lead-free perovskites were used for the first time to simultaneously detect H_2, H_2S, NH_3, and NO_2. Among them, the minimum detection limits of Cs_3CuBr_5 and $Cs_2AgBiBr_6$ for H_2, H_2S, NH_3, and NO_2 are 24.4/41.4 ppm, 13.6/52.4 ppm, 13.95/43.52 ppm, and 8.5/26.3 ppb, respectively. When detecting NO_2 at a relative humidity of 70%, the response of Cs_3CuBr_5 slightly decreases, while that of $Cs_2AgBiBr_6$ slightly increases, but both maintain good sensitivity. This is because the hydrophobicity of graphene protects the perovskites from decomposition and enhances their stability. Due to the fact that the electron-hole binding energy of perovskite nanocrystals is lower than the thermal energy, electron traps are generated, which in turn induce radiative recombination of carriers and promote interactions with target gases. When target gases come into contact with the perovskites, carriers accumulate in the perovskite nanocrystals, and an interface is formed between graphene and perovskites, which compensates for the carriers of lead-free perovskites and reduces the resistance level of the thin film. This study broadens the application of lead-free perovskites in gas sensing.

https://doi.org/10.2147/IJN.S554538

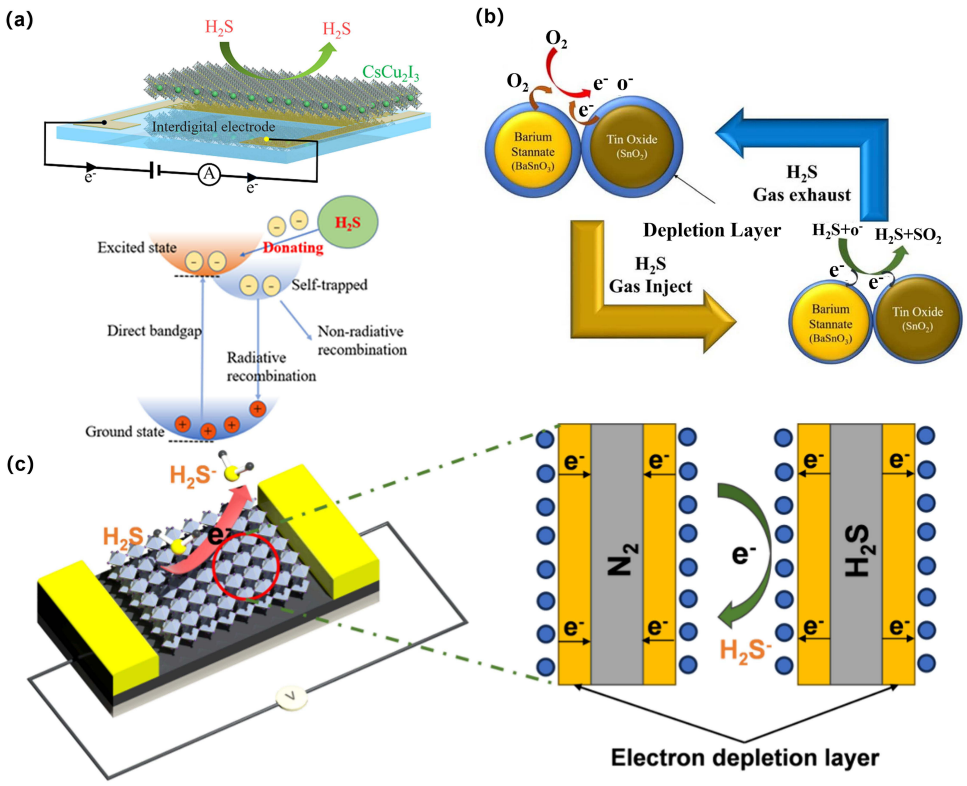

Figure 4 (**a**)gas-sensing mechanism of $CsCu_2I_3$ for H_2S gas.[34] (**b**) $SnO_2/BaSnO_3$ reaction of H_2S scheme.[12] (**c**) Mechanism diagram of H_2S gas sensor based on $Cs_2AgBiCl_6$ material.[37]

In addition, organic-inorganic composites also play an important role in the detection of H_2S gas. In 2024, Mao et al[38] synthesized a composite material composed of lead-free perovskite cesium-copper iodide nanocrystals ($CsCu_2I_3$) and a metal-organic framework (MOF-801) using an in-situ growth method. MOF-801 can act as a barrier to protect $CsCu_2I_3$. The sensor can detect H_2S gas in the concentration range of 0.005–100 μM, with a detection limit of 1.67 nM. This environmentally friendly composite material broadens the application scope of perovskites and provides a new pathway for their commercial development. In 2025, Li[12] et al synthesized lead-free perovskite $Cs_2AgBiCl_6$, which achieved an ultra-low detection limit of 5 ppb at room temperature and a sensitivity of 90.6 at 10 ppm, enabling highly sensitive H_2S detection. The sensing mechanism is based on charge transfer at the interface when H_2S molecules adsorb onto the surface of $Cs_2AgBiCl_6$, generating an internal electric field. Combined with the physical adsorption of H_2S molecules at Cl vacancies on the perovskite particles, the sensor's resistance changes, resulting in excellent gas-sensing performance. In the same year, Zhou[39] et al developed a $CsPbBr_3$ based-sensor with high sensitivity to H_2S at room temperature, achieving a detection limit of 200 ppb and a sensitivity of 4.76 at 5 ppm, and the gas-sensing performance still remains good even after six weeks. The high sensitivity stems from the formation of Pb-S bonds between H_2S and the perovskite, promoting the adsorption process and adjusting the perovskite's band structure. Also in 2025, Gao[40] et al employed a fully thermal evaporation method to synthesize $CsPbBr_3$ and deposited SnO_2 on the perovskite surface to form a heterojunction. The sensor based on this material exhibited a good response to H_2S, with an effective detection range of 1–200 ppm and a sensitivity of 1 at 100 ppm. The internal electric field of the heterojunction redistributed charges and enhanced surface sensitivity, while the SnO_2 coating prevents the intrusion of water and oxygen, thereby improving stability. Compared to solution-based methods, the thermally evaporated peperovskite gas sensor proposed in this study offers greater potential for large-scale sensor production. In 2025, Li[12] synthesized halide double perovskite $Cs_2AgBiCl_6$ is used for hydrogen H_2S detection. At an H_2S concentration of 400 ppb, the response and recovery times are 99.6s and 94.2s respectively, with a detection limit of 5 ppb for H_2S. After exposure to air for 30 days, the sensitivity shows little change. The sensor's moisture resistance test reveals that under relative humidity (RH) conditions of 11%,

33%, 54%, 75%, and 85%, the minimum detection limits are 40 ppb, 80 ppb, 80 ppb, 200 ppb, and 400 ppb respectively. The sensing mechanism involves the adsorption of H_2S by the perovskite, accompanied by changes in carrier concentration and charge transfer. This ultra-sensitive sensor is expected to enable early warning of H_2S leakage and early diagnosis of certain respiratory diseases in Figure 4b.

Oxide perovskites also show a high response to H_2S. In 2022, Hsu et al[41] prepared the $La_{0.8}Pb_{0.2}FeO_3$ perovskite and combined it with tungsten oxide (WO_3) to form a composite material. The WO_3/LPFO thin film based sensor exhibits a high response to H_2S. At the optimal temperature of 175 °C and a concentration of 1.25 ppm, the response rate is as high as 89.5%, and the response time is only 14s. Compared with WO_3, Pt-WO_3, and CuO-WO_3, it has a lower optimal working temperature and higher gas selectivity. WO_3 has poor gas selectivity and has high responses to both H_2S and NO_2. However, the response of WO_3/LPFO to NO_2 decreases significantly (from 107.9% to 3.5%), while the response to H_2S remains almost unchanged (from 99.5% to 89.5%), thus improving the selectivity for H_2S. In 2022, Wang et al[42] synthesized non-toxic two-dimensional nanosheets $NbWO_6$ with a thickness of only 1.5 nm. The sensor based on this material was tested in carbon monoxide, methanol, nitrogen dioxide, methane, ethanol, ammonia, acetone, toluene, and hydrogen sulfide, and it was found to have the highest selectivity for hydrogen sulfide (at 150 °C and a concentration of 0.5 ppm, the response-recovery time is 6/30s). When the gas is adsorbed on the nanosheet, a chemical reaction occurs between H_2S and $NbWO_6$. Since H_2S is a reducing gas, electrons flow from H_2S to $NbWO_6$, resulting in a change in resistance and a sensing effect. In 2023, Zheng[43] et al synthesized Fe/$LaCoO_3$ perovskite using a citric acid-assisted sol-gel method. Among the $LaFe_xCo_{1-x}O_3$ perovskite catalysts, the $LaFe_{0.4}Co_{0.6}O_3$ catalyst exhibited the highest H_2S conversion rate and 100% sulfur selectivity at 190°C. The doping of Fe facilitated the formation of oxygen vacancies and a macroporous structure, enhancing crystal mobility and physical adsorption efficiency. In 2024, Wei[44] et al developed a double perovskite, La_2FeMO_6, where the alternating substitution of Mn for Fe promoted the formation of asymmetric oxygen vacancies (Fe-V_o-Mn), improving H_2S conversion (>90%) and sulfur selectivity (nearly 100%). In the same year, Vu[37] et al combined nanofiber SnO_2 with perovskite $BaSnO_3$ to form a heterojunction thin film. Since both materials are n-type semiconductors, their contact interface generated defects, which trapped holes and electrons, increasing the electron density at the conduction band of $BaSnO_3$ and thereby enhancing sensitivity to H_2S. At 255°C, the composite maintained a sensitivity of 75±76% at 10 ppm H_2S, whereas pure SnO_2 exhibited a response rate of 63.15% under the same conditions in Figure 4c.

Detection of Ammonia

Ammonia (NH_3) is an alkaline gas that is relatively abundant in the atmospheric environmentand is also the major source of odorous pollutants. Currently, a significant amount of ammonia in the environment is directly or indirectly emitted by human activities, such as agricultural fertilization, industrial refrigeration, fertilizer production, livestock farming, vehicle exhaust, and a small amount from the ocean. Ammonia can be deposited in water bodies or soil with rainfall, thus damaging the ecological structure. At the same time, it can also adsorb on the surface of human skin, damaging human proteins and endangering human health. Ammonia is also an important marker for the detection of kidney and liver diseases. The average creatinine value of patients with chronic kidney disease (CKD) is 455.2±294.1 μmol/L, while that of healthy volunteers is 62.1±7.5 μmol/L. The range of ammonia exhaled by the CKD group is 3.32±2.19 ppm, and the ammonia exhaled by healthy people is 0.49±0.08 ppm.

In 2020, Li et al[45] synthesized a $MAPbBr_3$ sensor on a TiO_2 layer, which demonstrated a high response to ammonia. At a concentration of 5 ppm, the fluorescence intensity of the quantum dots increased by 72%, and at 100 ppm, the fluorescence intensity increased by 988%. In the same year, Jiao et al[46] synthesized the $(CH_3NH_3)PbBr_{3-x}I_x$ perovskite and tested its response to ammonia, acetone, and ethanol simultaneously. They found that the perovskite had good selectivity for ammonia. The specificity lies in that the perovskite undergoes physical adsorption with NH_3, forming van der Waals forces, and also undergoes a chemical reaction through cation replacement. However, the detection of ammonia by $(CH_3NH_3)PbBr_{3-x}I_x$ is irreversible in Figure 5. Subsequently, Li et al[47] deposited a $CH_3NH_3PbBr_3$ ($MAPbBr_3$) thin film on a GeO_2 substrate and covered it with tetrabutylammonium (TBA) ligands as a stabilizer. This material has strong luminescence ability, and in an ammonia environment, the fluorescence intensity decreased by 62.5%, with response-recovery times of 61s and 65s. The ammonia concentration in the range of 0–100 ppm has a linear

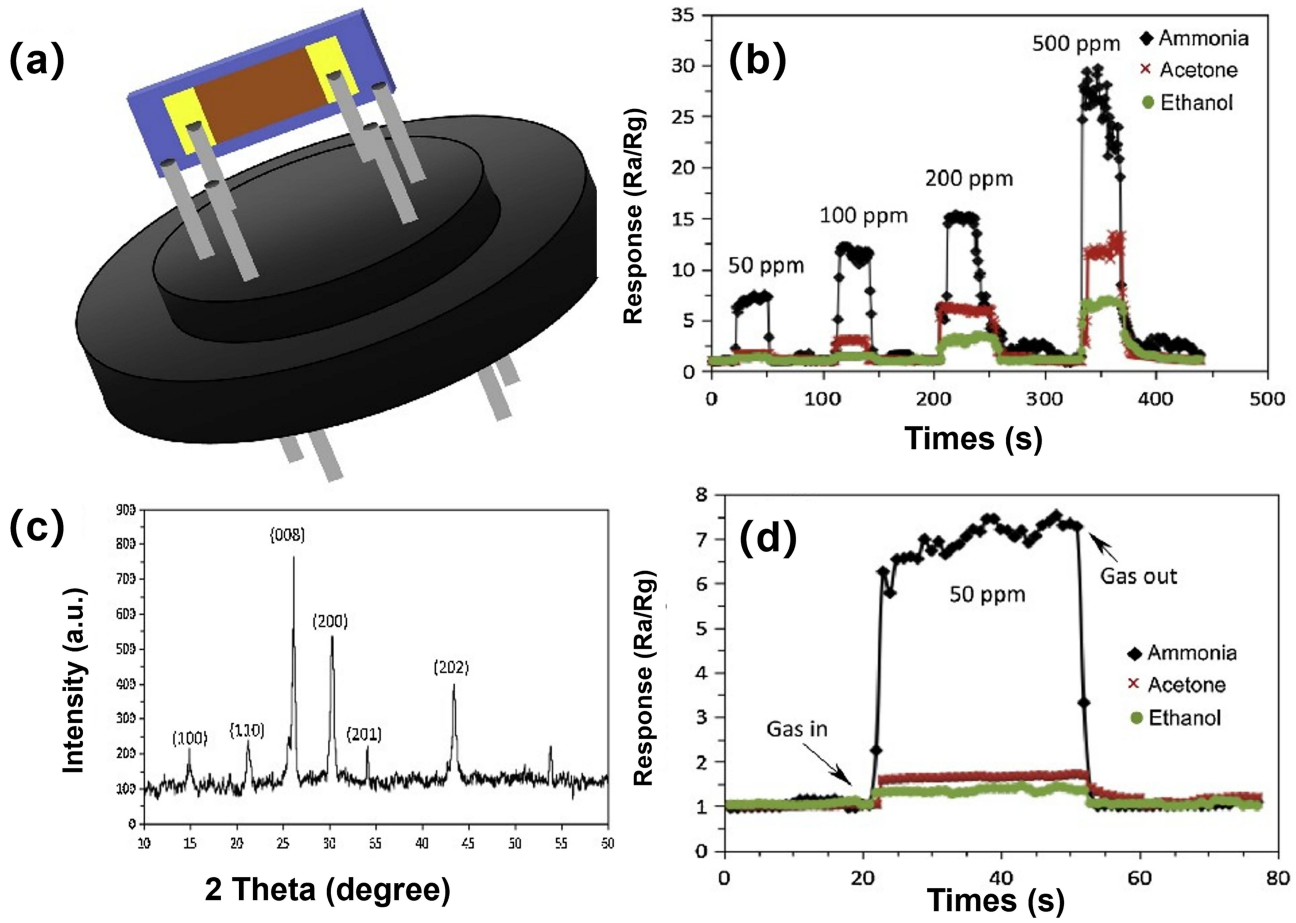

Figure 5 (**a**) Schematic diagram of the $MAPbBr_{3-x}I_x$ perovskite thin-film gas-sensing sensor (**b**) XRD pattern of the $MAPbBr_{3-x}I_x$ perovskite thin film. (**c**) Responses of the $MAPbBr_{3-x}I_x$perovskite thin-film sensor to ammonia, acetone, andethanol at different gas concentrations. (**d**) Partially enlarged details of Figure (**c**).[46]

relationship with PL, showing promising prospects in ammonia detection. In the same year, Maity et al[48] studied the excellent properties of ($CH_3NH_3PbI_3$/MAPI) perovskite, which has high selectivity and sensitivity to ammonia. The sensor is made of color-changeable cellulose paper and electrical sensing components and can detect ammonia below the ppm concentration level. They also compared sensors made of $MAPbBr_3$ and $FAPI_3$, and $MAPI_3$ had higher selectivity. When the $MAPI_3$-coated perovskite paper was exposed to 10 ppm of NH_3, the black color of the paper turned yellow within 10 seconds. However, this sensor is disposable, has a low service life, and is irreversible. In 2021, Sheikh et al[13] deposited a thin film on an FTO substrate using a single-step spin-coating method to fabricate a chloride-doped $MAPbI_3$ sensor $MAPbI_{3-x}Cl_x$. In an environment of 10 ppm ammonia, it had a response degree of 591%, which is 13 times that of pure $MAPbI_3$. The response-recovery times of the $MAPbI_3$ sensor (0.4s and 1.1s) were faster than those of the $MAPbI_{3-x}Cl_x$ sensor (0.7s and 1.4s) because $MAPbI_{3-x}Cl_x$ has a larger specific surface area and higher density. In the same year, Gui shun et al[49] reported a lead-free phenethyllammonium$_3Bi_2Br_9$ sensor. At a concentration of 30 ppm of NH_3, its sensitivity is 1.76, and the minimum detection limit is as low as 0.2 ppm. When NH_3 is introduced, NH_3 molecules are first adsorbed onto the phenethyllammonium$_3Bi_2Br_9$ thin film, and then they penetrate the film, causing the dissociation of the $Bi_2Br_9^{3-}$ double-octahedron and forming a new substance, NH_4Br, which in turn causes a change in resistance. In 2023, Li[50] et al pioneered the use of non-stoichiometric $MAPbI_3$ thin films for the detection of NH_3 and HCl. The excess PbI_2 in the films facilitated the formation of abundant iodine vacancies, thereby enhancing gas-sensing performance. The detection limits for NH_3 and HCl reached 0.08 ppm and 0.11 ppm, respectively. At a concentration of 10 ppm, the response values were 144% for NH_3 and −8% for HCl. In 2024, Maity et al[51] synthesized a textile-based organic lead-free halide perovskite sensor. The sensor was grown on textiles at low temperatures using $CH_3NH_3SnI_3$/

$MASnI_3$ as raw materials. The sensor can respond through color changes and electronic readings. When exposed to 100 ppm of ammonia gas, the original black color turns brown, and the maximum calibrated sensitivity of the sensor is 85%. The textile-based sensor can be used in wearable electronic products and is free from the harm of lead toxicity. In the same year, Kurniawan[52] for the first time fabricated $MAPbI_3$ perovskite films using a fractal electrode structure. The gas-sensing performance of the device with the Hilbert electrode design showed a maximum response value of 2.82 towards 10 ppm NH_3, which was 1.45 times higher than that of the traditional interdigital electrode (IDE) structure. Moreover, the gas-sensing performance remained good even after exposure to air for 12 days. Compared with the traditional IDE, the fractal electrode device exhibited better response performance. This is because the fractal electrode generates more corner points than the IDE structure, which leads to an increase in the electric field and thus a more significant gas-sensing effect. In 2025, Li[53] et al synthesized a two-dimensional perovskite material, BA_2PbBr_4 (butylammonium lead bromide), for NH_3 detection. This material exhibited high stability at room temperature, high sensitivity (41.4% response to 100 ppm NH_3), and fast response/recovery times (25/49s). The layered structure of BA_2PbBr_4 enhanced its stability, retaining 82.6% of its initial response after three weeks in Figure 6a and b. In the same year, Kassa[54] et al improved the

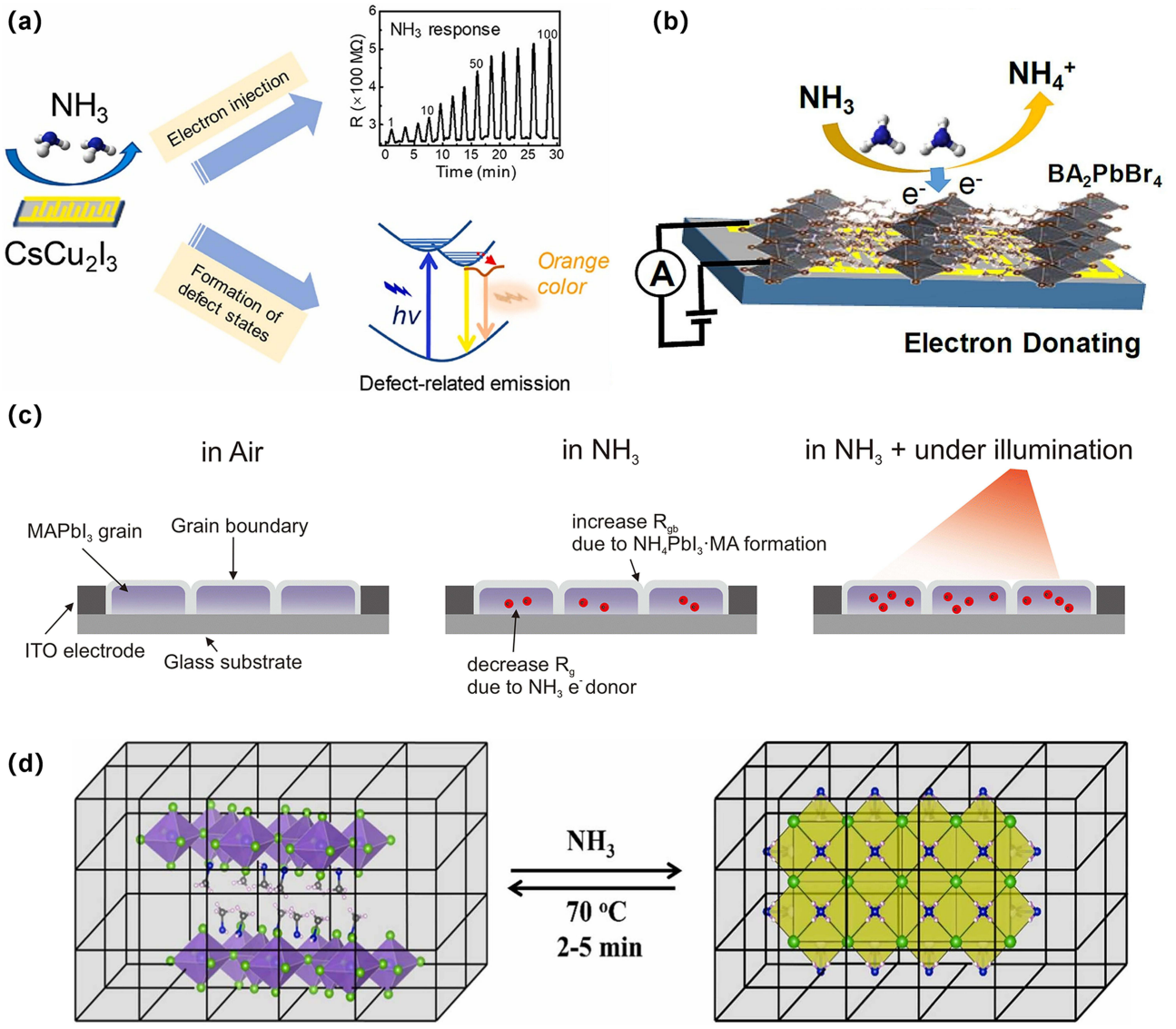

Figure 6 (**a**) Conffguration coordinate diagram of $CsCu_2I_3$ including STEs emission and defect-related emission.[53] (**b**) Schematic NH_3 sensing mechanism of BA2PbBr4[53] (**c**) Schematic illustration of the proposed NH_3 gas sensing mechanism in the $MAPbI_3$ film.[54] (**d**) Ammonia sensing mechanism of the MA_2SnBr_6 material.[55]

https://doi.org/10.2147/IJN.S554538

NH_3 response of $MAPbI_3$ by modulating its free electrons and holes through increased light intensity. Under 380 nm illumination at 100 W cm^{-2}, the sensor achieved a response of 3.99 to 10 ppm NH_3-324% higher than in dark conditions-demonstrating the great potential of light-assisted NH_3 detection using $MAPbI_3$ in Figure 6d. Also in 2025, Tiwari[55] et al developed a sensor based on MA_2SnBr_6-encapsulated $MACuBr_4$ with varying Sn/Cu ratios. In the presence of NH_3, the copper bromide salt decomposed, causing a color change from purple to greenish-yellow and altering electrical resistance. The encapsulation by MA_2SnBr_6 reduced Cu^{2+} leaching, improving stability. The sensor achieved a colorimetric detection limit of 5 ppm and an electrochemical detection limit of 1 ppm. At a Sn/Cu ratio of 0.77:0.23, the sensor maintained stable performance over 52 cycles of exposure to 50 ppm NH_3 in Figure 6c.

Inorganic halide perovskites are also commonly used for ammonia detection. In 2020, Huang et al[56] $CsPbBr_3$ quantum dot thin films were prepared, and their ammonia response was detected by means of dynamic passivation. Under 365nm ultraviolet light, the color change of the quantum dot thin films was observed upon ammonia introduction. It was found that the $CsPbBr_3$ thin film sensor showed a significant response to ammonia in the range of 25–350 ppm with a linear relationship, and the theoretical minimum limit could reach 8.85ppm, the stability of the film remained above 80% of its initial level after 130 hours. The reaction principle is that ammonia undergoes physical adsorption with $CsPbBr_3$ perovskite quantum dots, passivating the defects on their surface without destroying the structure of the quantum dots. Moreover, ammonia has a pair of lone pair electrons, which interact with surface lead atoms in Figure 7a. In 2021, Jiao et al[57] prepared $Cs_3Bi_2I_6Br_3$ for ammonia detection by the liquid spin-coating method. The sensor consists of disc-shaped particles vertically standing on the substrate and interpenetrating to form a continuous network. The maximum response value is 11.8–500 ppm, and the stability is as high as 14 days. It contains no heavy-

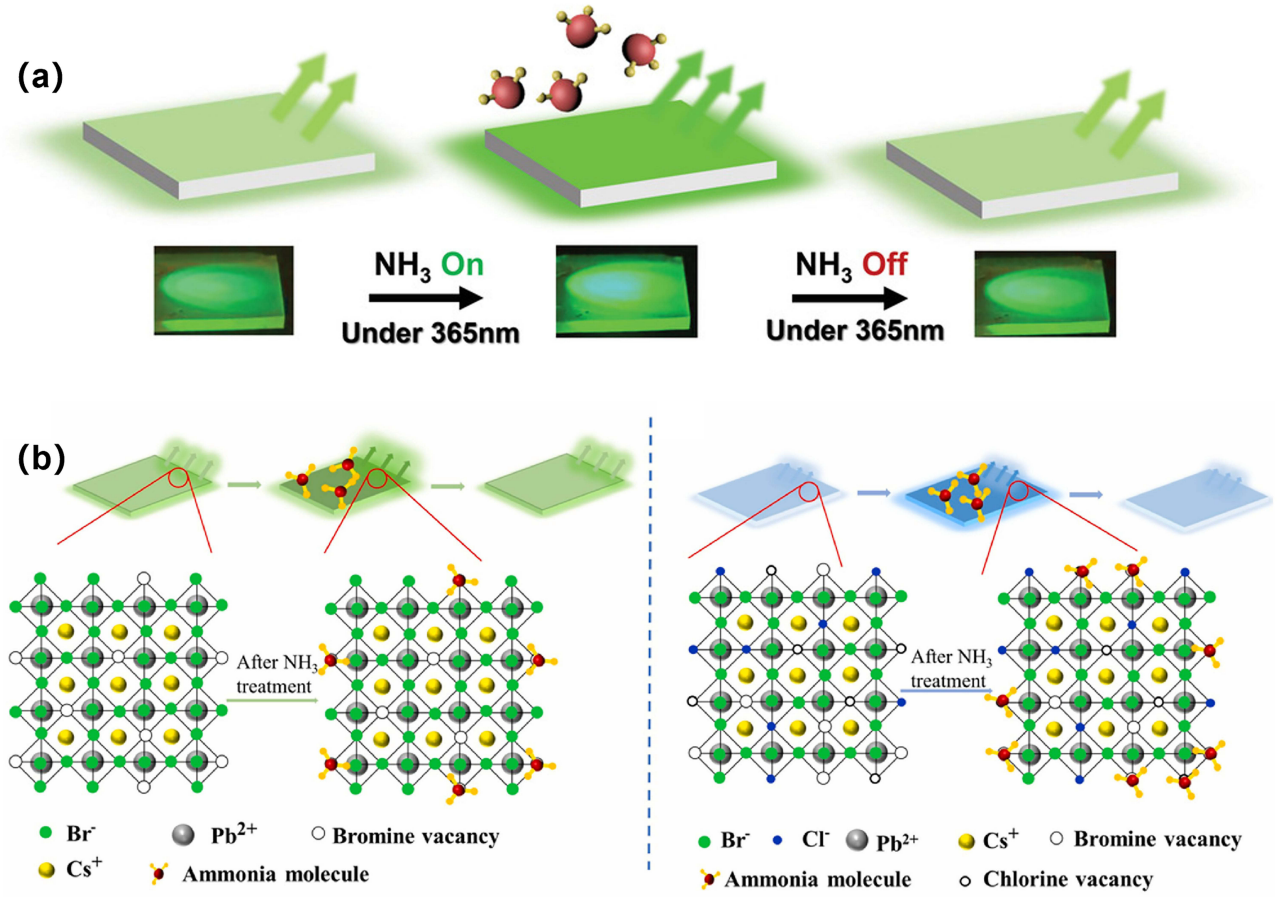

Figure 7 (**a**) Schematic diagram of the dynamic passivation response-recovery cycle of perovskite quantum dots.[56] (**b**) The passivation mechanism between ammonia molecules and the surface defects of $CsPbX_3$ quantum dots.[58]

metal lead, opening up new ideas for the design of green and environmentally friendly sensors. In 2022, Huang et al[58] prepared five types of cesium lead halide perovskite quantum dots with different halogen-ion ratios. Among them, only $CsPbBr_{1.5}I_{1.5}$, $CsPbBr_3$, and $CsPbBr_{1.5}Cl_{1.5}$ showed obvious sensing effects for ammonia. $CsPbBr_3$ has relatively few surface holes, so its response recovery time is short. When detecting ammonia at 50 ppm, the response and recovery times of $CsPbBr_3$ are 21s and 23s, those of $CsPbBr_{1.5}I_{1.5}$ are 55s and 50s, and those of $CsPbBr_{1.5}Cl_{1.5}$ are 66s and 67s. The passivation between $CsPbX_3$-type quantum dots and ammonia occurs because the lone-pair electrons in ammonia molecules form ammonia-lead ligands with uncoordinated lead ions. Electrons are transferred from ammonia to the quantum dots, resulting in physical adsorption. Therefore, lead-based perovskites are highly sensitive to ammonia in Figure 7b. In 2023, Huangfu et al[59] proposed a method for growing $CsPbBr_3$ nanocrystals on a polyvinylidene fluoride membrane for the first time. Under the protection of SiO_2, the $CsPbBr_3$ nanocrystals can still maintain 88.11% of their initial fluorescence intensity after being placed at room temperature for 104 days. The nanocrystals were made into test-paper sensors. Among several common harmful gas vapors (ammonia, toluene, ethyl acetate, methanol, ethanol, dichloromethane, acetic acid, chloroform, DMSO, DMF, acetaldehyde, acetone), only ammonia can greatly quench the fluorescence of the test paper. The $CsPbBr_3$-SiO_2 nanocomposite membrane can be used as a fluorescence sensor for high-concentration NH_3 based on the principle of fluorescence quenching. In the same year, Wu[60] et al synthesized Fe^{3+}-doped perovskite quantum dots ($CsPbBr_3$-QDs) embedded in a zeolite matrix via a hydrothermal method. The incorporation of trace Fe^{3+} effectively compensated for lead vacancy defects and significantly suppressed bromine loss, enabling the QDs to retain 98% of their original photoluminescence (PL) intensity after 100 days of air exposure-demonstrating dramatically enhanced stability. When exposed to NH_3, these quantum dots exhibited excellent response characteristics with high sensitivity. In 2024, Zheng et al[61] prepared a carboxyl-rich $Cs_3Cu_2I_5$-DES sensor. The minimum detection limit for NH_3 is 0.0642 ppm. DES has room-temperature curing properties and can be used as a supporting material for the $Cs_3Cu_2I_5$-DES thin film. The reaction principle is that NH_3 can be adsorbed and enriched on the surface of the $Cs_3Cu_2I_5$-DES thin film and react with the carboxyl groups on DES, resulting in a significant decrease in the fluorescence intensity of the $Cs_3Cu_2I_5$-DES thin film. There is a good linear relationship between the decrease in fluorescence intensity and the NH_3 concentration, which makes it possible to construct a new high-sensitivity NH_3 sensor. In the same year, Li[62] et al developed $CsCu_2I_3$ thin films for NH_3-triggered stimulus-responsive fluorescence anti-counterfeiting applications. Under 100 ppm ammonia exposure, the films demonstrated a response value of 2.07 with response/recovery times of 21/29 seconds. The sensing mechanism involves electron-donating NH_3 molecules interacting with the p-type perovskite, leading to reduced film conductivity. NH_3 adsorption creates high-density trap states in $CsCu_2I_3$ crystals, facilitating energy transfer from self-trapped exciton (STE) emission to defect-associated emission, resulting in bright orange luminescence.

Detection of Nitrogen Oxides

Nitric oxide plays an important role in the semiconductor, chemical engineering industries, and biology. However, nitric oxide (NO) is somewhat toxic and is easily oxidized to nitrogen dioxide (NO_2) in the air. The latter has stronger toxicity and corrosiveness. Symptoms of nitric oxide poisoning include headache, dizziness, general weakness, and coma[63] From the perspectives of environmental protection and human health, achieving highly sensitive detection of NO is of great research significance. In 2021, Chen et al[64] used Cs_2PtI_6 to achieve the first example of detecting NO with a lead-free halide perovskite. The detection concentration is as low as 100 ppb, and it has ultra-high selectivity for NO. It can operate at room temperature for more than two months. When Cs_2PtI_6 interacts with NO, the strong bonding between the Pt 5s and N 2s orbitals leads to a binding energy from Pt to NO of 0.72 eV and an electron transfer of 0.22 eV. Moreover, Cs_2PtI_6 can be made into flexible sensors, enabling wearable functions on the human body or clothing. In the same year, Chen et al[65] prepared the lead-free halide Cs_2TtI_6 perovskite. The specifically synthesized fern-like compound Cs_2TtI_6 has a minimum detection limit of 60 ppb, extremely high stability, and high NO selectivity. This is because there is a strong bonding between Te and N, forming a σ-bond, which can combine NO with Te^{4+}, resulting in a change in conductivity. This creates opportunities for the research of non-metallic perovskites. Currently, metal-oxide gas-sensing sensors are mainly used for highly sensitive detection of NO_2. However, their detection generally requires a high-temperature working environment, and their detection sensitivities at room temperature and low temperatures are

relatively low, which seriously hinders their practical application and development. Therefore, it is of great significance to develop sensing materials that are highly sensitive and reusable for NO_2 detection at room temperature.

In 2017, Zhang et al[66] used thiocyanate-ion (SCN^-)-doped organometallic halide perovskite $CH_3NH_3PbI_{3-x}(SCN)_x$ thin films as sensing materials and developed high-performance gas sensors. This simple chemiresistive sensor can sensitively and selectively detect acetone vapor and NO_2 gas, with detection limits of 20 ppm and 200 ppb.

In 2022, Lu et al[14] prepared a sensitive and ultrafast $FA_{0.83}Cs_{0.17}PbI_3$ perovskite sensor for NO_2 detection at room temperature. The detection limit is as low as 0.14 ppm, and it has good reversibility and selectivity. The response and recovery times for detecting 10 ppm of NO_2 are only 2s and 22s. The FACs thin film was placed in high-humidity air (50–60%) for 3 consecutive days without any morphological or structural changes, indicating its excellent stability and opening up a new path for NO_2 detection.

In addition, inorganic halide perovskites have also been studied for NO_2 detection. In 2021, Hung et al[67] studied the sensing performance of Cs_2SnI_6 for NO_2. First, a precursor solution was prepared by chemical vapor deposition (CVD), and then a Cs_2SnI_6 thin film was synthesized on a glass plate by a two-step method. The prepared sensor has a detection limit as low as 3 ppm. The response and recovery times of this sensor at room temperature for 20 ppm of NO_2 are 247s and 818s, respectively. The response of this sensor is affected by humidity. When the relative humidity (RH) increases from 0 to 52%, the sensing response slightly increases, and then it rapidly decreases after 75% RH. This is because at high humidity, as the response to NO_2 increases, more electrons enter the perovskite thin film, generating more e^- and O_2^-. Then, as more and more water molecules are adsorbed, the number of adsorption sites decreases, resulting in a rapid decrease in the response to NO_2. In the same year, Hung et al[68] studied the gas-sensing effect of Cs_2TeI_6 on NO_2 under 450-nm blue-light illumination. The detection limit is as low as 25 ppb. The higher the concentration of NO_2, the higher the response. The response degree is 0.87% at 25 ppb and 4.36% at 1000 ppb. Under laser illumination, the resistance value of the Cs_2TeI_6 thin film rapidly decreases from 1.6×10^{11} β to 3.9×10^9 β. The photo-response speed is fast, and the response/recovery time is 60/100 ms. The decrease in resistance is due to the generation of a large number of carriers inside the Cs_2TeI_6 thin film under blue-light illumination. Therefore, Cs_2TeI_6 is a promising material for nitrogen-dioxide gas sensors. In the same year, Sun[69] et al developed a nano-network gas sensor based on $CsCu_2I_3$, which demonstrated remarkable performance in NO_2 detection. The device showed response/recovery times of 146/413s at 50 ppb NO_2 concentration, maintained 60.2% response at 30 ppb, achieved a detection limit as low as 20 ppb, and exhibited excellent gas selectivity. The all-inorganic perovskite structure, free from weak organic bonds, displayed outstanding room-temperature stability and recyclability in Figure 8a. In 2024, Li[15] et al fabricated Cl-vacancy-rich $Cs_2AgInCl_6$ perovskite grown on TiO_2 nanotube arrays. This sensor showed a sensitivity of 7.26 to 1 ppm NO_2 at room temperature, with rapid response/recovery times of 38s and 59s respectively, and an ultra-low detection limit of 20 ppb. The sensing mechanism relies on Cl vacancies serving dual functions as both electron traps and active reaction sites. These defect sites effectively reduce the energy barrier for charge transfer, thereby accelerating electron exchange with NO_2 molecules in Figure 8b. In the same year, Ahmed et al[70] studied the sensitivity of the $RbSnCl_3$ perovskite to NO gas using density-functional theory. The adsorption energy of $RbSnCl_3$ for NO is-0.56 eV, and the recovery time is between 3.4×10^{-8} and 3.5×10^{-8} s. The strong adsorption energy and extremely short recovery time make $RbSnCl_3$ a potential candidate for detecting NO. In 2025, Kim[71] and others prepared flexible perovskite $CsCu_2I_3$, which exhibits excellent gas sensing performance towards NO_2. At a concentration of 5 ppm, the sensitivity is as high as 1509%, and it can be fully recovered with good repeatability. Moreover, it can detect extremely low concentrations of NO_2 (1.16 ppb). Through first-principles calculations, NO_2 can interact with Cs and I atoms on the surface. A total of four adsorption sites are selected, namely the top site and the bridge site for each atom in Figure 8c. In the same year, Wang[72] and others prepared a sensor with a sandwich structure, $Cs_2AgBiBr_6/SnO_2/ZnO$ nanorods. With SnO_2 serving as a hole blocking agent, it can not only facilitate the transfer of electrons but also improve the stability. Additionally, the coating of SnO_2 enhances the polarization effect of the ZnO nanorods, effectively increasing the chemical adsorption rate and significantly improving the sensing performance. The response to 100 ppm of NO_2 is 9.66, and the response and recovery times are 8/9s, with the lowest detection limit at 500 ppb.

In addition, organic-inorganic hybrid perovskites have also been studied in this regard. In 2022, Duong[73] and others fabricated a mixed-dimensional 2D/3D organic-inorganic metal perovskite (OIMHP) sensor, which has a sensitivity of

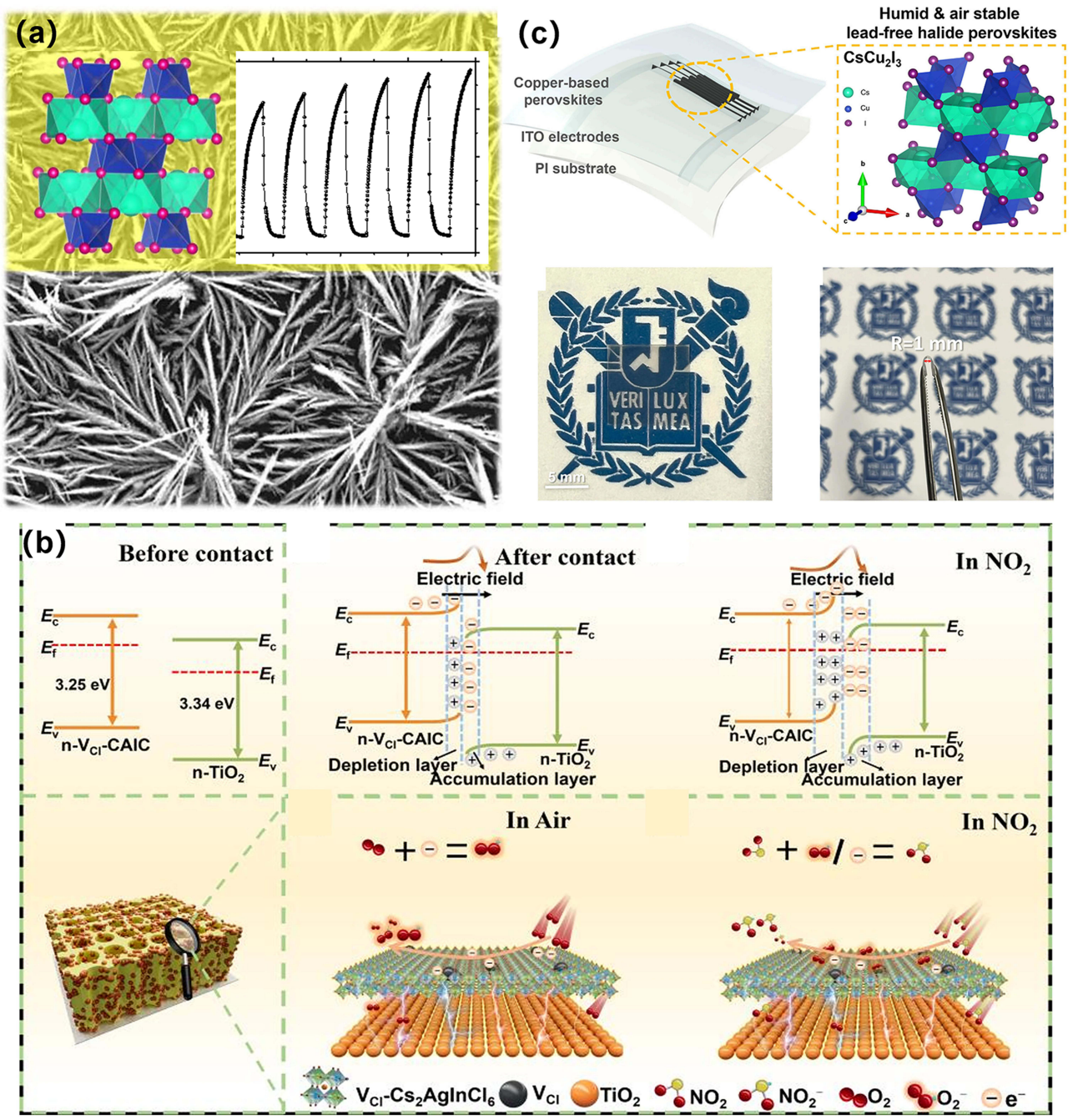

Figure 8 (**a**) The crystal structure diagram of the $CsCu_2I_3$. Dynamic resistance response of the perovskite $CsCu_2I_3$ nanostructured networks sensor to 20 ppb NO_2 measured at room temperature. SEM image of the as-prepared $CsCu_2I_3$ nanostructured networks with high density grown on an IDE/SiO_2/Si substrate.[69] (**b**) Change in the energy band of VCl-CAIC/TiO_2 NTs heterojunctions (before contact, in air, and after exposure to NO_2). Charge transfer process of VCl-CAIC/TiO_2 NTs heterojunctions.[15] (**c**)A schematic illustration of a nontoxic lead-free, transparent, and flexible halide perovskite $CsCu_2I_3$gas sensor.[71]

6.3±0.83 towards 1 ppm of NO_2, as well as fast response and recovery times (5.7s and 12.7s respectively). The high sensitivity can be attributed to the formation of a NO_2 2D layer on the surface of the 3D perovskite, which increases the interaction between the NO_2 gas and the amino groups in both the 3D and 2D perovskites. In 2025, Ye[74] and others prepared a covalent organic framework (COF) coating on the surface of the inorganic perovskite Cs_2PdBr_6. TAPB-PDA@ Cs_2PdBr_6 can detect 10 ppb of NO_2, which is the lowest value reported for perovskite-based gas sensors, and the performance remains stable after several weeks. It surpasses the selectivity and sensitivity of traditional halide perovskite sensors.

https://doi.org/10.2147/IJN.S554538

Detection of Carbon Dioxide

Due to the massive consumption of fossil fuels and the excessive emission of CO_2, the resulting greenhouse effect and energy shortage have seriously affected global climate change, becoming a major challenge faced by the world.[75]

In 2019, Liu et al[76] prepared Mn-doped $CsPb(Br/Cl)_3$ mixed-halide perovskites by the thermal-injection method and made some modifications. Under the visible-light illumination of a filter, it can be used as a catalyst for photocatalytic CO_2 reduction. When reacting with CO_2, the yields of CO and CH_4 change significantly. The optimal yields reach 1917 μmol g^{-1} and 82 μmol g^{-1}, respectively, which are 14.2 and 1.4 times those of $CsPbBr_3$, providing new ideas for improving the efficiency of photocatalytic CO_2 reduction.

In 2020, Zhao et al[77] designed and explored copper-based halide perovskite $CsCuCl_3$ and its corresponding Br-substituted sample ($CsCuCl_2Br$) as catalysts for photocatalytic CO_2 reduction for the first time. $CsCuCl_3$ has a satisfactory bandgap (1.92 eV) and conduction-band minimum (CBM), which can absorb sunlight and drive the conversion of CO_2 to CH_4 and CO. The Br^- substitution can not only narrow the bandgap but also promote the transport of carriers, providing a new way for the design and synthesis of efficient lead-free perovskite photocatalysts. In 2023, Li[16] and others developed $CsPb_{1-x}Er_xBr_3$ perovskite, which can be used for CO_2 detection. The detection principle is based on the tunable mid-infrared emission of $CsPb_{1-x}Er_xBr_3$ perovskite glass at 2700–2800 nm. The infrared light source of the perovskite glass can be more compatible with the infrared characteristic absorption peak of CO_2. In 2025, Chen et al[78] synthesized $Cs_3Bi_2Br_9$ perovskite (abbreviated as CBB) on BiOBr via the isovalent ion exchange method. The nanosheets of BiOBr microspheres not only provide abundant CO_2 adsorption sites but also prevent the aggregation of CBB nanoparticles. The photocatalytic CO production rate based on this material reaches 0.224 μmol·h^{-1}. This work not only offers a new approach for the synthesis of bismuth-based perovskites but also opens up a new system for the efficient reduction of carbon dioxide using perovskites.

In 2024, Ye[17] and others synthesized three types of two-dimensional hybrid double perovskites (2D HDPs) using long-chain alkylammonium cations of different sizes, namely $(BA)_4AgBiBr_8$, $(HA)_4AgBiBr_8$, and $(OA)_4AgBiBr_8$. These materials exhibit both high sensitivity and stability in chemiresistive CO gas sensing: specifically, $(BA)_4AgBiBr_8$ achieves a detection limit of 20 ppb for CO and maintains its performance even after continuous exposure to ambient air for 270 days, while the experimental detection limits of $(HA)_4AgBiBr_8$ and $(OA)_4AgBiBr_8$ are 80 ppb and 120 ppb, respectively. The core structural feature of 2D HDPs is the "perovskite inorganic layers sandwiching large hydrophobic layers". This structure can effectively block water molecule erosion, enhancing environmental stability, but slightly weakens the interaction between gas molecules and the perovskite surface. Their sensing response stems from the semiconductor properties and the interaction between CO and active sites: the ionic lattice of perovskites promotes the adsorption of CO at point defects through acid-base interactions, which further triggers the transfer of electrons from CO to the perovskite, and ultimately changes the material's resistivity to generate a sensing signal. This breakthrough lays a foundation for practical applications in environmental monitoring, safety systems, and disease diagnosis, significantly enhancing the application.

Detection of VOCs

VOC_s is the abbreviation of Volatile Organic Compounds. The World Health Organization defines VOCs as volatile organic compounds with a melting point below room temperature and a boiling point between 50–260 °C[79] Exposure to low-concentration VOCs may cause symptoms such as a sore throat, irritated and teary eyes, swollen and painful nose, and even nosebleeds and skin allergies. More seriously, it can cause nausea, vomiting, and breathing difficulties. Long-term exposure to VOCs can also damage the liver, nervous system, immune system, etc.

In 2021, Zhu et al[80] synthesized $(C_4H_9NH_3)_2PbI_4$ single crystals and performed density-functional calculations on the adsorption energies of gases such as C_2H_5OH, C_6H_6, CH_2Cl_2, HCHO, CH_3COCH_3, and C_7H_8. They found that the single crystal has high selectivity for p-xylene. The sensing principle is the adsorption-desorption process. When p-xylene molecules encounter $(C_4H_9NH_3)_2PbI_4$, the electron-transfer process leads to a change in carrier transport, thus changing its resistance and causing the gas sensor to respond to p-xylene.

In the same year, Huang[18] et al synthesized $MAPbBr_3$ perovskite nanocrystals and prepared a fluorescence sensor for detecting methylamine with a hydrophobic PVDF layer. Protected by the hydrophobic PVDF layer, the sensor can still be used after two months of storage and can maintain more than 90% of its initial PL intensity, showing excellent stability. The nanofibers have a dual-mode sensor response to 5–200 ppm of MA gas, with a detection limit (LOD) of 0.8 ppm. In 2025, Li[81] and others synthesized a sensor composed of Eu-MOFs-$MAPbBr_3$ perovskite nanocrystals, which exhibits excellent gas sensing performance towards methylamine gas. There is a good linear relationship when detecting methylamine gas within the concentration range of 9–90 ppm, and the detection limit can be as low as 1 ppm. This material maintains nearly constant fluorescence intensity after being kept in an environment of 20 °C and 70% atmospheric humidity for 15 days.

In addition, inorganic perovskites have also been studied for VOCs detection. In 2022, Xuan et al[19] prepared $CsPbBr_3$ nanocrystals coated with metal oxide ZnO for detecting heptanal in air and artificial breath. The sensor has good sensitivity (S = 0.36) and short response/recovery times (36.5s/5.3s) to 200 ppm of heptanal in air, and the detection limit in air can reach 2 ppm. The maximum concentration of heptanal in the breath of healthy people is 8.9 ppm, and the concentration of heptanal in lung-cancer patients is often higher, indicating that an abnormal increase in heptanal levels is related to lung-cancer lesions. This research opens up a new path for the diagnosis of lung cancer.

In the same year, Xu et al[82] optimized the $CsPbBr_3$-ZnO composite material, prepared a $CsPbBr_3$-MPA/ZnO heterostructure, and found that it has a high response to ethanolamine. At room temperature, the response to 100 ppm of ethanolamine (EA) is 13.23, and the response time is only 50s. This is because MPA containing short-chain thiol ligands could effectively promote the migration of carriers from ZnO to $CsPbBr_3$, improving the carrier utilization rate of the $CsPbBr_3$-MPA/ZnO composite material and thus enhancing the sensitivity to EA, the repeatability remains stable for more than one month. In the same year, Xu[83] and others fabricated a composite sensor based on $CsPbBr_3$@MoS_2, which shows a sensitive response to ethanolamine (EA): the sensitivity is 29.87 at 100 ppm EA, with good repeatability and stability, and the theoretical limit of detection (LOD) is approximately 21 ppb; under relative humidity (RH) conditions of 13%, 43%, 53%, and 65%, the responses to 50 ppm EA are 12.57, 6.68, 5.49, and 4.44, respectively. The sensing mechanism is as follows: oxygen molecules are chemisorbed on the surface of $CsPbBr_3$ nanocrystals to form O^{2-} ions. When exposed to an EA atmosphere, EA molecules react with the chemisorbed O^{2-} ions, releasing electrons that are injected into the depletion layer. This reduces the barrier energy ($\Delta\Phi$), thereby lowering the resistance of the sensor. Moreover, the specific surface area of $CsPbBr_3$ nanoblocks reaches 24.851 m^2/g, which facilitates the adsorption of gas molecules and surface reactions.

In 2023, Yang[20] and others synthesized the composite perovskite material $Cs_4PbBr_6/CsPbBr_3$ for the detection of 2,4-dinitrophenylhydrazine. There is a linear relationship for 2,4-dinitrophenylhydrazine within the concentration range of 0.05–30 mg/L, with $R^2 = 0.995$, and the detection limit is 0.033 mg/L. This study indicates that $Cs_4PbBr_6/CsPbBr_3$ shows great potential to be developed into a quantitative detection method for hydrazine substances. In the same year, Xu[84] and others prepared a nitrobenzene sensor based on the hydrophilic perovskite nanocomposite $CsPbBr_3$/TDPA. This sensor has a good linear relationship for nitrobenzene within the concentration range of 1–0.1 μM, and the lowest limit is 0.05 μM. Moreover, the inorganic material has excellent stability and repeatability. This study broadens the application of perovskite sensors in the field of electrochemistry. In the same year, Xu[85] and others prepared the composite material Ag@$SnO_2/CsPbBr_3$ for the detection of low-concentration ethanolamine at room temperature. Ag@SnO_2 can promote the directional transport of carriers, and Ag@$SnO_2/CsPbBr_3$ has a large specific surface area; both factors can enhance the gas-sensing performance of the quantum dots. Over 28 days of long-term stability testing, the sensitivity remained around 40. The theoretical minimum detection limit for ethanolamine at room temperature is 44.43 ppb, realizing continuous and efficient monitoring of ethanolamine in Figure 9a and 9b. In 2024, Wang[86] and others synthesized the three-dimensional organic-inorganic hybrid perovskite $FASnI_3/SnO_2$, which exhibits excellent gas-sensing performance towards formaldehyde, with a theoretical detection limit as low as 200 ppb. It also has high moisture resistance: when the humidity is 78%, the response value to 50 ppm formaldehyde remains 32.5. The long-term stability was tested for 30 days, and excellent gas-sensing performance was consistently demonstrated. $(BA)_2SnI_4$ leads to the formation of heterojunctions and more oxygen vacancies. $FASnI_3/(BA)_2SnI_4$ is hydrophobic, which can improve the stability and moisture resistance of gas sensing in Figure 9c. In 2024, Shi[87] and others studied a composite gas sensor based on

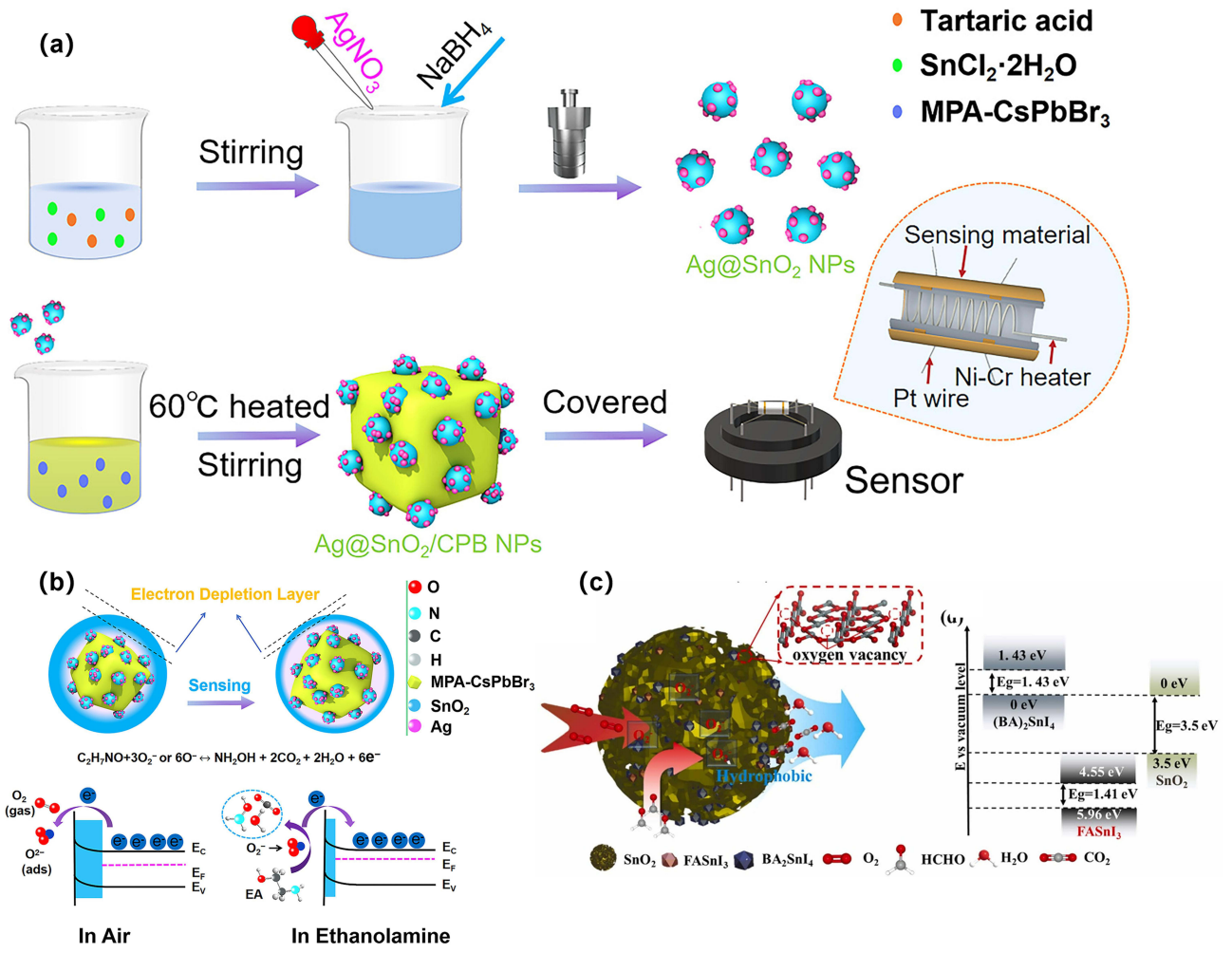

Figure 9 (**a**)The preparation process of Ag@SnO_2/$CsPbBr_3$.[85] (**b**)Schematic diagram of 2Ag@SnO_2/ $CsPbBr_3$ sensing mechanism.[85] (**c**) The sensing mechanism for FA^+ 10BA-S sensor to trace HCHO and Energy level of conduction band and valence band for sensitive material.[86]

$CsPbBr_3$@In_2O_3, which exhibits excellent sensitivity, reproducibility, and stability towards triethylamine (TEA): at 60 °C, its sensitivity to 100 ppm TEA reaches 52.92, and the gas-sensing performance remains good even after exposure to air for 13 days. This composite material has a mesoporous structure and a high specific surface area. When exposed to TEA, TEA reacts with O^{2-} ions and releases electrons into the conduction band of In_2O_3, leading to a decrease in the resistance of the sensor. Table 1 summarizes the sensing properties of perovskite-sensitive materials and their devices in recent years, providing a reference basis for the further rational design of halide perovskite gas sensors.

Reaction Principles of Perovskite Materials for Detecting Target Gases

Surface Adsorption and Chemical Reaction

Halide perovskites possess a large specific surface area and high surface reactivity, enabling them to effectively adsorb target gas molecules. Once adsorbed onto the perovskite surface, these gas molecules may undergo chemical reactions with the material, resulting in changes to its electronic structure. For instance, oxidizing gases such as NO_2 can extract electrons from the perovskite surface, reducing the electron concentration and thereby increasing the material's resistance. Conversely, reducing gases such as H_2 or NH_3 can inject electrons into the perovskite surface, increasing the electron concentration and decreasing the resistance. These electronic structure changes, triggered by gas adsorption and chemical reactions, allow for the detection of target gases-both their presence and concentration-by monitoring variations in electrical properties such as resistance.

Table 1 Halide Perovskite Sensitive Materials and Their Gas Sensing Properties

Detected Substance	Sensing Material	Limit of Detection	Response Time	Recovery Time	Reference
H_2S	$FAPbBr_3$ nanoparticles	500ppb	12s	36s	[31]
	$MAPbI_{3-x}(SCN)_x$ film	200ppb	23s	56s	[32]
	$CsBr$-$Cs_3Bi_2Br_3I_6$ nanoplates	500ppb	33s	45s	[33]
	$CsCu_2I_3$ film	200ppb	67s	45s	[34]
	$Bio(s\text{-}pea)_2CsPb_3Br_7$ nanocrystals film				[35]
	$CsPbBr_3$-Fe_2O_3 nanocrystals film	0.27ppb	1.84s	24.2s	[36]
	Cs_3CuBr_5 nanocrystals film	13.6ppm			[11]
	$Cs_2AgBiBr_6$ nanocrystals film	52.4ppm			[11]
	$CsCu_2I_3$-MOF nanocrystal film	1.67 nM			[38]
	$Cs_2AgBiCl_6$ particles	5ppb	99.6s	94.2s	[12]
	$CsPbBr_3$ powders film	200ppm	73.5s		[39]
	SnO_2/$CsPbBr_3$ nanocrystals film	1 ppm	26s	56.3s	[40]
	$WO_3/La_{0.8}Pb_{0.2}FeO_3$ nanosheets	1.25ppm			[41]
	$NbWO_6$ nanosheets	0.5ppm	6s	30s	[42]
	$LaFe_{0.4}Co_{0.6}O_3$ nanoparticles				[43]
	La_2FeMO_6 gel				[44]
	$SnO_2/BaSnO_3$ nanofibers	2ppm	82s	235s	[37]
NH_3	Tio_2-$MAPbBr_3$ film	920ppb	7s	73s	[45]
	$(CH_3NH_3)PbBr_{3-x}I_x$ film	7.5ppm			[46]
	GeO_2-$MAPbBr_3$ film	0.46ppm			[47]
	$MAPbI_3$ microcube film	500ppb	11s	8s	[48]
	$MAPbI_{3-x}Cl_x$ film		0.7s	1.4s	[13]
	Phenylethylammoniu-$m_3Bi_2Br_9$ film	200ppb	39s	130s	[49]
	$MAPbI_3$ film	80ppb	29s	11s	[50]
	$MASnI_3$ textile-based film	5ppm			[51]
	$MAPbI_3$ film	100ppb			[52]
	BA_2PbBr_42D film	10ppm	25s	49s	[53]
	$MAPbI_3$ film	0.1ppm			[54]
	MA_2CuBr_4/MA_2SnBr_6 film	1ppm			[55]
	$CsPbBr_3$ PQD film	8.85ppm	10s	30s	[56]

(*Continued*)

https://doi.org/10.2147/IJN.S554538

Table 1 (Continued).

Detected Substance	Sensing Material	Limit of Detection	Response Time	Recovery Time	Reference
	$Cs_3Bi_2I_6Br_3$ film	11.8ppm	20s	120s	[57]
	$CsPbBr_3$ PQD film	20ppm	21s	23s	[58]
	$CsPbBr_{1.5}I_{1.5}$ PQD film	20ppm	55s	50s	[58]
	$CsPbBr_{1.5}Cl_{1.5}$ PQD film	20ppm	66s	67s	[58]
	$CsPbBr_3$-SiO_2 nanocrystals film	2160ppm			[59]
	$CsPbBr_3$/Fe PQD film				[60]
	$Cs_3Cu_2I_5$-DES nanocrystals film	0.0642 ppm			[61]
	$CsCu_2I_3$ film	1ppm	21s	29s	[62]
	Cs_3CuBr_5 nanocrystals film	13.95ppm			[11]
	$Cs_2AgBiBr_6$ nanocrystals film	43.52ppm			[11]
NO	Cs_2PtI_6 nano-power	100ppb	160s	314s	[64]
	Cs_2TeI_6 Fern-like	60ppb	138s	152s	[65]
	$RbSnCl_3$ film		3.4×10^{-8}s	3.5×10^{-8}s	[70]
NO_2	$CH_3NH_3PbI_{3-x}(SCN)_x$ film	200ppb			[66]
	$FA_{0.83}Cs_{0.17}PbI_3$ film	140ppb	2s	22s	[14]
	Cs_2SnI_6 film	3ppm	247s	818s	[67]
	Cs_2TeI_6 film	25ppb	60ms	100ms	[68]
	$CsCu_2I_3$ nanoneedle film	20ppb	146s	413s	[69]
	$Cs_2AgInCl_6$ nanocrystals	20ppb	38s	59s	[15]
	$CsCu2I_3$ film	1.16ppb			[71]
	$Cs_2AgBiBr_6/SnO_2$/ZnO film	500ppb	8s	9s	[72]
	OIMHP three-dimensional (3D)		5.7s	12.7s	[73]
	TAPB-PDA-Cs_2PdBr_6 nanospheres film	10 ppb			[74]
	Cs_3CuBr_5 nanocrystals film	8.5ppb			[11]
	$Cs_2AgBiBr_6$ nanocrystals film	26.3ppb			[11]
CO_2	Mn-$CsPb(Br/Cl)_3$ film				[76]
	$CsCuCl_3$ film				[77]
	$CsPb_{1-x}Er_xBr_3$ rare earth perovskites				[16]
	$Cs_3Bi_2Br_9$/BiOBr nanoparticles				[78]
CO	$(BA)_4AgBiBr_8$ 2D HDP	20 ppb			[17]
	$(HA)_4AgBiBr_8$ 2D HDP	80ppb			[17]
	$(OA)_4AgBiBr_8$2D HDP	120ppb			[17]
Xylene	$(C_4H_9NH_3)_2PbI_4$ single crystal film				[80]

(*Continued*)

Table 1 (Continued).

Detected Substance	Sensing Material	Limit of Detection	Response Time	Recovery Time	Reference
Methylamine	$MAPbBr_3$ nano-fibers	0.8ppm			[18]
	Eu-MOFs-$MAPbBr_3$ nanocrystals film	1ppm	20s		[81]
Heptanal	ZnO-$CsPbBr_3$ PQD film	2ppm	36.5s	5.3s	[19]
Ethanolamine	$CsPbBr_3$-MPA/ZnO nanoparticles film	100ppm	50s	78s	[82]
	CsPbBr3@MoS power	21ppb			[83]
	Ag@SnO_2/$CsPbBr_3$ nanoparticles	44.43ppb	67s	787s	[84]
Nitrobenzene	$CsPbBr_3$/TDPA nanocrystals film	0.05 Mm			[20]
Formaldehyde	$FASnI_3$/SnO_2 2D/3D nanocrystals	200ppb	67s	81s	[85]
Triethylamine	$CsPbBr_3$@In_2O_3 PQD film				[86]

Changes in Optical Properties

Halide perovskites exhibit unique optical properties, with their absorption spectra, fluorescence spectra, and other optical characteristics being susceptible to the presence of target gases. When target gas molecules interact with the perovskite material, they may alter its energy band structure, defect states, and other electronic properties, thereby influencing its optical behavior. For instance, the adsorption of certain gases can lead to the quenching or enhancement of the perovskite's fluorescence. By monitoring changes in the material's optical properties-such as variations in fluorescence intensity or absorption spectra-detection of target gases can be achieved. A significant change in fluorescence intensity, for example, can serve as an indicator of the presence and concentration variations of the target gas.

Ion Migration and Diffusion

In halide perovskites, ions such as halide ions possess a certain degree of mobility. When target gas molecules come into contact with the perovskite material, they may either promote or inhibit ion migration and diffusion. Such changes in ion migration and diffusion can significantly affect the material's electrical properties, including conductivity. For instance, the interaction between specific gas molecules and the perovskite surface may alter the migration pathways or rates of halide ions, thereby inducing changes in the material's conductivity. By measuring these conductivity variations, the presence and concentration of the target gas can be effectively detected.

Surface Plasmon Resonance Effect (SPR)

In some cases, halide perovskite materials can interact with target gases, triggering the surface plasmon resonance effect. Surface plasmon resonance refers to the resonant phenomenon generated by the collective oscillation of free electrons in metal or semiconductor nanostructures when interacting with incident light. When target gas molecules are adsorbed on the surface of the perovskite material, they alter properties of the material such as the dielectric constant, thereby affecting the conditions for surface plasmon resonance. By detecting changes in parameters related to surface plasmon resonance (eg, resonance wavelength, resonance intensity), highly sensitive detection of target gases can be achieved. Provide a schematic diagram summarizing the reaction mechanism above, as shown in Figure 10.

Challenge and Prospects

With the rapid development of nano-chemical technology, gas sensors based on perovskite materials have made significant progress in recent years. This review provides an overview of recent advancements in perovskite-based gas-sensitive materials and gas sensor devices, summarizing relevant research from both material and device

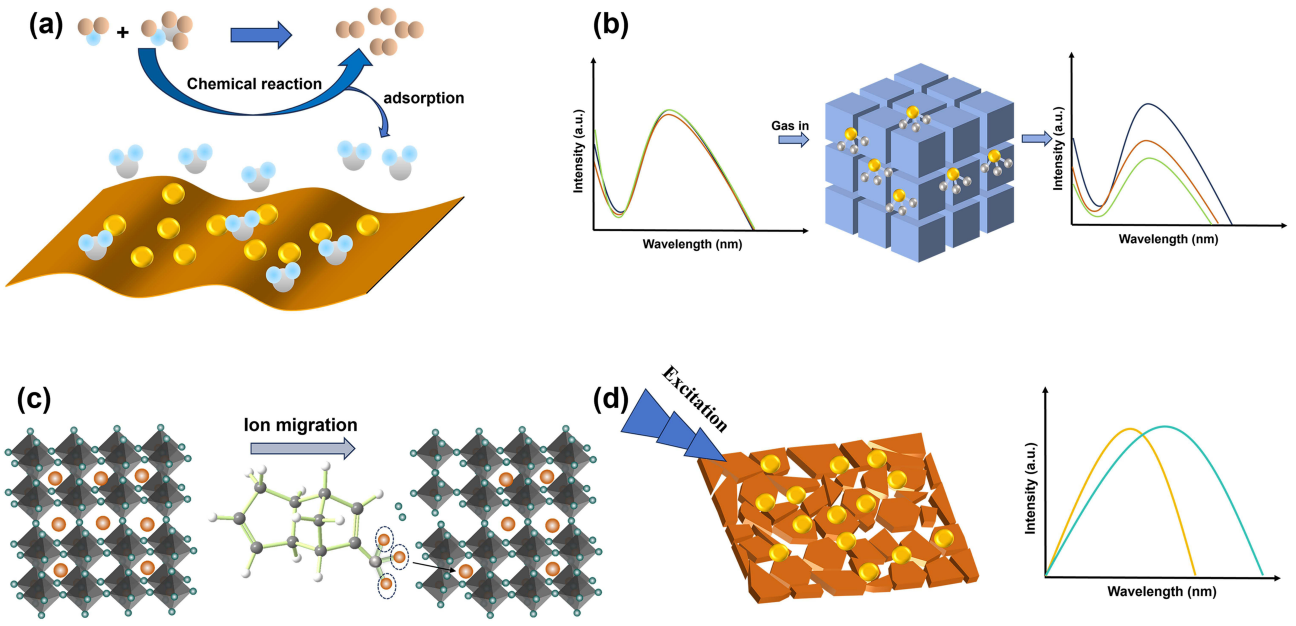

Figure 10 (**a**) Surface Adsorption and Chemical Reaction (**b**) Changes in Optical Properties(**c**) Ion Migration and Diffusion(**d**) Surface Plasmon Resonance Effect.

perspectives. Perovskite-based gas sensors have demonstrated remarkable performance, including low optimal operating temperatures, cost-effectiveness, high sensitivity, and superior gas-sensing properties. Nevertheless, challenges remain in improving the stability and reproducibility of these materials. Additionally, their selectivity in complex gas mixtures and multi-cycle reusability require further enhancement, while the presence of lead (Pb) in traditional perovskites poses substantial environmental and health risks that severely hinder commercialization. To address these challenges, future research should focus not only on the doping of noble and transition metals and the development of composite materials but also on the synthesis of unique micro- and nanostructured perovskite materials with enhanced gas-sensing properties-among which lead-free perovskites have emerged as a pivotal and promising direction.

The prospect of lead-free perovskites in gas sensing is increasingly prominent, driven by their environmental benignity and tunable functional properties that align with the core demands of next-generation sensing technologies. Representative systems such as tin-based perovskites (TPSCs) and all-inorganic $CsCu_2I_3$ perovskites have showcased remarkable potential. These materials inherently resolve the heavy metal pollution issue of traditional lead-based perovskites, removing a key barrier to commercialization. Current research efforts in perovskite-based gas sensing are primarily focused on four key directions, with lead-free systems becoming a central focus. Firstly, investigating single-crystal lead-free perovskite structures could further unlock superior optoelectronic properties and enhanced sensing performance, building on the high carrier mobility and defect tolerance of these materials. Secondly, deepening the understanding of ion-electron coupling mechanisms in lead-free systems will enable rational design of doped/substituted ions to improve structural stability, sensing response, and repeatability-critical for overcoming intrinsic limitations like tin oxidation in TPSCs. Thirdly, developing effective encapsulation strategies remains critical for enhancing moisture resistance, complementing the inherent stability of all-inorganic lead-free perovskites. Finally, combining selectively designed lead-free perovskites with micro/nano-fabrication techniques and advanced signal processing algorithms will accelerate the development of multiplexed sensor arrays, particularly valuable for applications such as closed-cabin environmental monitoring and wearable IoT devices where low toxicity and multi-analyte discrimination are essential.

These interconnected approaches collectively advance the field toward robust, high-performance, and eco-friendly gas-sensing solutions. We believe that research on lead-free perovskite gas sensors will soon achieve clear breakthroughs through scientific theoretical design and rational preparation methods, leveraging synergies between material innovation and device engineering. Ultimately, we are optimistic about the development of lead-free perovskite gas sensors, as they not only address the core challenges of traditional perovskite sensors but also align with global environmental

sustainability goals, promising to meet the diverse needs of future commercialization in environmental monitoring, healthcare, and smart IT.

Acknowledgments

This work was supported by Program of Shanghai Academic Research Leader (22XD1404700), Shanghai Industrial Collaborative Innovation Project (XTCX-KJ-2023-49), National Natural Science Foundation of China (NSFC) Youth Program (No:82302118) and National Postdoctoral Fellowship Program (B) (No:GZB20230991).

Disclosure

The authors declare no conflicts of interest.

References

1. Fei H, Lingling W, Wei C, Yin H, Fen Z, Wei S. Hydrohalide perovskite sensitive materials and their gas sensing applications. *J Silicate Materi*. 2024;52(01):292–304. doi:10.14062/j.issn.0454-5648.20230259
2. Zhang P, Cheng J, Lu Y, et al. Hypersensitive MR angiography based on interlocking stratagem for diagnosis of cardiac-cerebral vascular diseases. *Nat Commun*. 2023;14(1):6149. doi:10.1038/s41467-023-41783-9
3. Li W, Li J, Gao J, et al. The fine-tuning of thermosensitive and degradable polymer micelles for enhancing intracellular uptake and drug release in tumors. *Biomaterials*. 2011;32(15):3832–3844. doi:10.1016/j.biomaterials.2011.01.075
4. Lee J, Ryu J, Yoon S, et al. Introducing additives to metal halide perovskites based on luminescent mechanisms. *Coord Chem Rev*. 2025;542:216858. doi:10.1016/j.ccr.2025.216858
5. Ding J, Zhang G, Dai H, Chen H, Fu H. Gas sensor preparation based on green biological template: a review. *Sens Actuators A*. 2024;366:115051. doi:10.1016/j.sna.2024.115051
6. Wang H, Kim DH. Perovskite-based photodetectors: materials and devices. *Chem Soc Rev*. 2017;46(17):5204–5236. doi:10.1039/c6cs00896h
7. Getachew G, Wibrianto A, Rasal AS, et al. Lead-free metal halide perovskites as the rising star in photocatalysis: the past, present, and prospective. *Pro Mater Sci*. 2023;140:101192. doi:10.1016/j.pmatsci.2023.101192
8. Getachew G, Tien Y-C, Kan T-C, et al. Defect-passivated metal halide perovskite quantum dots stabilized into biodegradable porous polydopamine nanoparticles for photothermal/chemodynamic/gas therapy of cancer. *Chem Eng J*. 2023;467:143560. doi:10.1016/j.cej.2023.143560
9. Getachew G, Wibrianto A, Rasal AS, Batu Direrssa W, Chang J-Y. Metal halide perovskite nanocrystals for biomedical engineering: recent advances, challenges, and future perspectives. *Coord Chem Rev*. 2023;482:215073. doi:10.1016/j.ccr.2023.215073
10. Getachew G, Korupalli C, Rasal AS, Direrssa WB, Fahmi MZ, Chang J-Y. Highly luminescent, stable, and red-emitting $CsMgxPb_{1-x}I_3$ quantum dots for dual-modal imaging-guided photodynamic therapy and photocatalytic activity. *ACS Appl Mater Interfaces*. 2022;14(1):278–296. doi:10.1021/acsami.1c19644
11. Casanova-Chafer J, Garcia-Aboal R, Atienzar P, Llobet E. Unraveling the gas-sensing mechanisms of lead-free perovskites supported on graphene. *ACS Sens*. 2022;7(12):3753–3763. doi:10.1021/acssensors.2c01581
12. Li M, Ye W, Ruan J, et al. Lead-free halide double perovskite $Cs_2AgBiCl_6$ for H_2S trace detection at room temperature. *ACS Sens*. 2025;10(3):2224–2233. doi:10.1021/acssensors.4c03532
13. Sheikh AD, Vhanalakar VK, Katware AS, Pawar KK, Kulkarni SK. Ultrasensitive organic-inorganic nanotube thin films of halogenated perovskites as room temperature ammonia sensors. *J Alloy Compd*. 2022;894:162388. doi:10.1016/j.jallcom.2021.162388
14. Lu Z, Lou C, Cheng A, Zhang J, Sun J. A sensitive and ultrafast $FA_{0.83}Cs_{0.17}PbI_3$ perovskite sensor for NO_2 detection at room temperature. *J Alloy Compd*. 2022;919:165831. doi:10.1016/j.jallcom.2022.165831
15. Li K, Wang H, He Z-K, Song -Y-Y, Gao Z, Zhao C. Engineering Cl vacancies in lead-free halide double perovskites decorated on TiO_2 nanotubes for highly sensitive NO_2 sensing at room temperature. *Chin Chem Lett*. 2025;36(8):110610. doi:10.1016/j.cclet.2024.110610
16. Li C, Zhang X, Li L, et al. Local crystal field-induced tunable mid-infrared luminescence of $CsPb_{1-x}Er_xBr_3$ perovskite fluoride glasses and applied to the detection of CO_2 in hydrogen energy. *Ceram Int*. 2023;49(17, Part A):27815–27826. doi:10.1016/j.ceramint.2023.05.270
17. Ye W, Lin H-Z, Li M, Jiang L, Chen D, Lu J-M. Dimensional reduction in $Cs_2AgBiBr_6$ enables long-term stable Perovskite-based gas sensing. *Nat Commun*. 2025;16(1):4820. doi:10.1038/s41467-025-60206-5
18. Huang G, Zhou Y, Li F, et al. An effective and reliable fluorescent sensor for selective detection of methylamine gas based on in-situ formation of $MAPbBr_3$ perovskite nanocrystals in electrospun fibers. *Sens Actuators B*. 2021;347:130618. doi:10.1016/j.snb.2021.130618
19. Xuan W, Shan H, Hu D, et al. In-situ synthesis of stable ZnO-coated $CsPbBr_3$ nanocrystals for room-temperature heptanal sensors. *Mater Today Chem*. 2022;26:101155. doi:10.1016/j.mtchem.2022.101155
20. Yang M, Yan Y, Liu E, Sun Q, Fan J. Temperature-dependent $Cs_4PbBr_6/CsPbBr_3$ perovskite composite for sensing 2,4-dinitriphenylhydrazine. *Mater Res Bull*. 2023;160:112135. doi:10.1016/j.materresbull.2022.112135
21. Sessolo M, Gil-Escrig L, Longo G, Bolink HJ. Perovskite Luminescent Materials. *Top Curr Chem*. 2016;374(4):52. doi:10.1007/s41061-016-0051-1
22. Kim TW, Park N-G. Methodologies for structural investigations of organic lead halide perovskites. *Mater Today*. 2020;38:67–83. doi:10.1016/j.mattod.2020.03.025
23. Perumal Veeramalai C, Feng S, Zhang X, Pammi SVN, Pecunia V, Li C. Lead–halide perovskites for next-generation self-powered photodetectors: a comprehensive review. *Photonics Res*. 2021;9(6):968–991. doi:10.1364/PRJ.418450
24. Sadhukhan P, Roy A, Sengupta P, et al. The emergence of concentrator photovoltaics for perovskite solar cells. *Appl Phys Rev*. 2021;8(4). doi:10.1063/5.0062671
25. Zhang C, Qian L, Zeng W. MOS based gas sensor in detection of volatile organic compounds: a review. *Sens Actuators A*. 2025;393:116818. doi:10.1016/j.sna.2025.116818

26. Cao X, Yang C, Zhu X, et al. Synergistic enhancement of chemotherapy for bladder cancer by photothermal dual-sensitive nanosystem with gold nanoparticles and PNIPAM. *Chin Chem Lett*. 2024;35(8):109199. doi:10.1016/j.cclet.2023.109199
27. Xiao C, Ma Z, Gao X, Zou P, Jia L. Fabrication of Pt functionalized $LaFeO_3$ porous structures for highly sensitive detection of formaldehyde. *Sens Actuators B*. 2024;410:135644. doi:10.1016/j.snb.2024.135644
28. Souri M, Salar Amoli H. Gas sensing mechanisms in ABO_3 perovskite materials at room temperature: a review. *Mater Sci Semicond Process*. 2023;156:107271. doi:10.1016/j.mssp.2022.107271
29. Feng X, Liu B, Zhou Z, et al. Engineering hierarchical metal-organic@metal-DNA heterostructures for combinational tumor treatment. *Nano Res*. 2023;16(11):12633–12640. doi:10.1007/s12274-023-5909-2
30. Yao C, Jingchao T, Yaquan L, Ting Z. The hazards, causes, and treatment methods of hydrogen sulfide in offshore oil fields. *Petrol Refin Technol*. 2022;29(12):194–196.
31. Ayesh AI, Alghamdi SA, Salah B, Bennett SH, Crean C, Sellin PJ. High sensitivity H_2S gas sensors using lead halide perovskite nanoparticles. *Results Phys*. 2022;35:105333. doi:10.1016/j.rinp.2022.105333
32. Lee K-Y, Hsieh J-C, Chen C-A, et al. Ultrasensitive detection of hydrogen sulfide gas based on perovskite vertical channel chemo-sensor. *Sens Actuators B*. 2021;326:128988. doi:10.1016/j.snb.2020.128988
33. Zhang H, Zhang L, Zhao Z, et al. A sensitive $CsBr/Cs_3Bi_2Br_3I_6$ heterostructure perovskite gas sensor for H_2S detection at room temperature with high stability. *Sens Actuators B*. 2024;403:135238. doi:10.1016/j.snb.2023.135238
34. Ou K, Wang Y, Zhang W, et al. Highly sensitive H_2S gas sensor based on a lead-Free $CsCu_2I_3$ perovskite film at room temperature. *ACS Omega*. 2023;8(50):48326–48335. doi:10.1021/acsomega.3c07694
35. Zhang J, Yuan Z, Wang C, et al. Aqueous-phase dual-functional chiral perovskites for hydrogen sulfide (H_2S) detection and antibacterial applications in Escherichia coli. *J Colloid Interface Sci*. 2024;661:740–749. doi:10.1016/j.jcis.2024.01.207
36. Huang S, Shan H, Xu Y, Zuo J, Zhao Y, Gu X. Preparation of $CsPbBr_3@Fe_2O_3$ heterojunction nanocrystals for ppb-level H_2S sensing. *Ceram Int*. 2024;50(14):25607–25612. doi:10.1016/j.ceramint.2024.04.295
37. Vu T-N, Li Y-S, Hsu K-C, et al. Enhanced H_2S gas sensing performance of $SnO_2/BaSnO_3$ heterostructures. *ECS J Solid State Sci Technol*. 2024;13 (12):127001. doi:10.1149/2162-8777/ad9952
38. Mao M, Zu Y, Zhang Y, et al. Photoelectrochemical sensor for H_2S based on a lead-free perovskite/metal-organic framework composite. *Anal Chem*. 2024;96(10):4290–4298. doi:10.1021/acs.analchem.4c00041
39. Zhou K, Yang H, Du Z, et al. Ultrahigh selectivity H_2S gas sensor based $CsPbBr_3$ perovskites via Pb-S bonding interaction. *ACS Sens*. 2025;10 (1):517–525. doi:10.1021/acssensors.4c02980
40. Gao D, Shan H, Xu X, et al. Efficient all-thermally evaporated perovskite/metal oxide heterojunction for room-temperature hydrogen sulfide sensor. *J Alloy Compd*. 2025;1021:179784. doi:10.1016/j.jallcom.2025.179784
41. Hsu K-C, Chen B-D, Fang T-H, Hsu C-M. $WO_3/La_{0.8}Pb_{0.2}FeO_3$ perovskite heterostructure for highly active and selective hydrogen sulfide detection. *Ceram Int*. 2023;49(2):2236–2243. doi:10.1016/j.ceramint.2022.09.191
42. Wang J, Ren Y, Liu H, et al. Ultrathin 2D $NbWO_6$ perovskite semiconductor based gas sensors with ultrahigh selectivity under low working temperature. *Adv Mater*. 2022;34(2):e2104958. doi:10.1002/adma.202104958
43. Zheng X, Li B, Shen L, et al. Oxygen vacancies engineering of Fe doped $LaCoO_3$ perovskite catalysts for efficient H_2S selective oxidation. *Appl Catal B*. 2023;329:122526. doi:10.1016/j.apcatb.2023.122526
44. Wei Z, Jiang G, Wang Y, et al. Asymmetric oxygen vacancies in La_2FeMO_6 double perovskite for boosting oxygen activation and H_2S selective oxidation. *Chin J Catal*. 2024;62:198–208. doi:10.1016/S1872-2067(24)60051-3
45. Li G, She C, Zhang Y, et al. A "Turn-on" fluorescence perovskite sensor based on $MAPbBr_3$/mesoporous TiO_2 for NH_3 and amine vapor detections. *Sens Actuators B*. 2021;327:128918. doi:10.1016/j.snb.2020.128918
46. Jiao W, He J, Zhang L. Synthesis and high ammonia gas sensitivity of $(CH_3NH_3)PbBr_{3-x}I_x$ perovskite thin film at room temperature. *Sens Actuators B*. 2020;309:127786. doi:10.1016/j.snb.2020.127786
47. Li G, Zhang W, She C, et al. Stable fluorescent NH_3 sensor based on $MAPbBr_3$ encapsulated by tetrabutylammonium cations. *J Alloy Compd*. 2020;835:155386. doi:10.1016/j.jallcom.2020.155386
48. Maity A, Mitra S, Das C, Siraj S, Raychaudhuri AK, Ghosh B. Universal sensing of ammonia gas by family of lead halide perovskites based on paper sensors: experiment and molecular dynamics. *Mater Res Bull*. 2021;136:111142. doi:10.1016/j.materresbull.2020.111142
49. Li G, Zhang Y, Zhao X, et al. Bismuth-based lead-free perovskite film for highly sensitive detection of ammonia gas. *Sens Actuators B*. 2021;345:130298. doi:10.1016/j.snb.2021.130298
50. Li G, Hou G, Zhang X, et al. Non-stoichiometric hybrid halide perovskite film for gaseous NH_3 and HCl sensing. *New J Chem*. 2023;47 (27):12541–12545. doi:10.1039/D3NJ02003G
51. Maity A, Mitra S, Ghosh B. Textile based lead-free halide perovskite $CH_3NH_3SnI_3$ ammonia gas sensor working at room temperature. *ACS Appl Electron Mater*. 2024;6(4):2677–2682. doi:10.1021/acsaelm.4c00230
52. Kurniawan A, Lee -C-C, Saputra R, et al. Improving the gas sensing performance of halide perovskite $MAPbI_3$ film via fractal geometry electrode structure. *Sens Actuators B*. 2024;417:136091. doi:10.1016/j.snb.2024.136091
53. Li G, Wu D, Wu X, Ge C. 2D halide perovskite BA_2PbBr_4 as a resistive gas sensor for reversible NH_3 detection. *Mater Lett*. 2025;389:138345. doi:10.1016/j.matlet.2025.138345
54. Kassa EE, Kurniawan A, Wu Y-F, Biring S. Achieving high response of perovskite-based ($MAPbI_3$) NH_3 gas sensors using binary mixed solvent approaches. *Sens Actuators A*. 2025;383:116116. doi:10.1016/j.sna.2024.116116
55. Tiwari A, Arjumand M, Vinay S, Yella A. Enhancing MA_2CuBr_4 ammonia sensors by overcoming Cu^{2+} reduction with MA_2SnBr_6 encapsulation. *J Alloy Compd*. 2025;1022:179942. doi:10.1016/j.jallcom.2025.179942
56. Huang H, Hao M, Song Y, Dang S, Liu X, Dong Q. Dynamic passivation in perovskite quantum dots for specific ammonia detection at room temperature. *Small*. 2020;16(6):e1904462. doi:10.1002/smll.201904462
57. Jiao W, He J, Zhang L. Fabrication and investigation of a new all-inorganic lead free perovskite $Cs_3Bi_2I_6Br_3$ for ammonia detection at room temperature. *J Alloy Compd*. 2022;895:162561. doi:10.1016/j.jallcom.2021.162561
58. Huang Y, Zhang J, Zhang X, et al. The ammonia detection of cesium lead halide perovskite quantum dots in different halogen ratios at room temperature. *Opt Mater*. 2022;134:113155. doi:10.1016/j.optmat.2022.113155

59. Huangfu C, Wang Y, Wang Z, Hu Q, Feng L. A stable and humidity resistant NH_3 sensor based on luminous $CsPbBr_3$ perovskite nanocrystals. *Talanta*. 2023;253:124070. doi:10.1016/j.talanta.2022.124070
60. Wu W, Zhao C, Hu M, Pan A, Xiong W, Chen Y. $CsPbBr_3$ perovskite quantum dots grown within Fe-doped zeolite X with improved stability for sensitive NH_3 detection. *Nanoscale*. 2023;15(12):5705–5711. doi:10.1039/d2nr06923g
61. Zheng Q, Zhou Y, Huang J, et al. $Cs_3Cu_2I_5$ perovskite nanocrystals embedded in room temperature curable deep eutectic solvents for sensing NH_3 gas. *J Alloy Compd*. 2024;986:174155. doi:10.1016/j.jallcom.2024.174155
62. Li G, Zhang Y, Xie J, et al. Ammonia-sensitive halide $CsCu_2I_3$ film for gas sensor and stimuli-responsive anti-counterfeiting. *Talanta*. 2025;281:126794. doi:10.1016/j.talanta.2024.126794
63. Zhao Z, Wang Z, Zheng C, Jin G, Shen X, Wu L. VTe_2 nanospheres for NO_2 gas sensors. *Sens Actuators A*. 2024;379:115935. doi:10.1016/j.sna.2024.115935
64. Chen ZK, Ye W, Lin HZ, Yu C, He JH, Lu JM. Lead-free halide Cs_2PtI_6 perovskite favoring pt-n bonding for trace NO detection. *ACS Sens*. 2021;6(10):3800–3807. doi:10.1021/acssensors.1c01791
65. Chen Z-K, Ye W, Wang J, Yu C, He J-H, Lu J-M. Sensitive NO detection by lead-free halide Cs_2TeI_6 perovskite with Te-N bonding. *Sens Actuators B*. 2022;357:131397. doi:10.1016/j.snb.2022.131397
66. Zhuang Y, Yuan W, Qian L, Chen S, Shi G. High-performance gas sensors based on a thiocyanate ion-doped organometal halide perovskite. *Phys Chem Chem Phys*. 2017;19(20):12876–12881. doi:10.1039/C7CP01646H
67. Hung PT, Hoat PD, Nguyen T-A, et al. Growth and NO_2 sensing properties of Cs_2SnI_6 thin film. *Mater Res Bull*. 2022;147:111628. doi:10.1016/j.materresbull.2021.111628
68. Hoat PD, Yun Y, Park B, et al. Synthesis of Cs_2TeI_6 thin film and its NO_2 gas-sensing properties under blue-light illumination. *Scr Mater*. 2022;207:114305. doi:10.1016/j.scriptamat.2021.114305
69. Sun X, Yang J, Wu Z, et al. Lead-free $CsCu_2I_3$ perovskite nanostructured networks gas sensor for selective detection of trace nitrogen dioxide at room temperature. *IEEE Sens J*. 2021;21(13):14677–14684. doi:10.1109/JSEN.2021.3071744
70. Ahmed MT, Roy D, Roman AA, Islam S, Ahmed F. A first principles study of $RbSnCl_3$ perovskite toward NH_3, SO_2, and NO gas sensing. *Nanoscale Adv*. 2024;6(4):1218–1226. doi:10.1039/D3NA00927K
71. Kim SJ, Nam GB, Kim YJ, et al. Ambient stable $CsCu_2I_3$ flexible gas sensors for reliable NO_2 detection at room temperature. *Nano Lett*. 2025;25(7):2894–2902. doi:10.1021/acs.nanolett.4c06149
72. Wang S, Hu H, Tan T, et al. Enhancing NO_2 sensing performance through interface engineering in $Cs_2AgBiBr_6/SnO_2$/ZnO-NRs sensor. *Sens Actuators B*. 2025;422:136654. doi:10.1016/j.snb.2024.136654
73. Duong T, John AT, Chen H, et al. Mixed-dimensional organic–inorganic metal halide perovskite (OIMHP) based gas sensors with superior stability for NO_2 detection. *Mater Adv*. 2022;3(2):1263–1271. doi:10.1039/D1MA00976A
74. Ye W, Li M, Li G, et al. Covalent organic framework-enhanced metal halide perovskites for selective and sensitive gas sensing. *Adv Funct Mater*. 2025;35(14):2418897. doi:10.1002/adfm.202418897
75. Rath RJ, Naficy S, Giaretta J, et al. Chemiresistive sensor for enhanced CO $_2$ gas monitoring. *ACS Sens*. 2024;9(4):1735–1742. doi:10.1021/acssensors.3c01779
76. Liu Y-W, Guo S-H, You S-Q, et al. Mn-doped $CsPb(Br/Cl)_3$ mixed-halide perovskites for CO_2 photoreduction. *Nanotechnology*. 2020;31(21):215605. doi:10.1088/1361-6528/ab72be
77. Zhao H-B, Liao J-F, Teng Y, Chen H-Y, Kuang D-B. Inorganic copper-based halide perovskite for efficient photocatalytic CO_2 reduction. *ACS Appl Mater Interfaces*. 2022;14(38):43354–43361. doi:10.1021/acsami.2c12695
78. Chen J, Zhang Q, Song J, et al. In situ synthesis of lead-free perovskite $Cs_3Bi_2Br_9$/BiOBr Z-scheme heterojunction by ion exchange for efficient photocatalytic CO_2 reduction. *J Catal*. 2025;442:115874. doi:10.1016/j.jcat.2024.115874
79. Zhao Z, Lei C, Liang T, et al. Multi-channel MEMS-FAIMS gas sensor for VOCs detection. *Micromachines*. 2023;14(3):608. doi:10.3390/mi14030608
80. Zhu M-Y, He P, Yang X-L, et al. DFT calculation on p-xylene sensing mechanism of $(C_4H_9NH_3)_2PbI_4$ single crystal based on physisorption. *Rare Met*. 2021;40(6):1571–1577. doi:10.1007/s12598-020-01606-y
81. Li Y, Tan X, Wu S, et al. Dual-emission ratiometric fluorescence sensor based on in situ formation of $MAPbBr_3$ perovskite nanocrystals in europium metal-organic frameworks for detection of methylamine gas. *Sens Actuators B*. 2025;426:137092. doi:10.1016/j.snb.2024.137092
82. Xu X, Wang X, Liu W, et al. Ambient stable $CsPbBr_3$/ZnO nanostructures for ethanolamine sensing. *ACS Appl Nano Mater*. 2022;5(10):15030–15041. doi:10.1021/acsanm.2c03227
83. Xu X, Wang S, Chen Y, et al. $CsPbBr_3$-based nanostructures for room-temperature sensing of volatile organic compounds. *ACS Appl Mater Interfaces*. 2022;14(34):39524–39534. doi:10.1021/acsami.2c09586
84. Zhang W-X, Chen J-S, Liu X-P, Mao C-J, Jin B-K. An electrochemiluminescent sensor based on hydrophilic $CsPbBr_3$/TDPA nanocrystals for sensitive detection of nitrobenzene. *Sens Diagn*. 2023;2(2):445–456. doi:10.1039/D3SD00007A
85. Xu X, Jiang H, Liu W, et al. Ag@SnO_2/$CsPbBr_3$ nanocomposite gas sensor for well-behaved low-concentration ethanolamine sensing at room temperature. *J Appl Phys*. 2024;135(8). doi:10.1063/5.0188699
86. Wang O, Zhang X, Kong J, et al. Fabrication of 2D/3D organic-inorganic hybrid perovskite derived materials and its low temperature response to formaldehyde at high humidity. *Sens Actuators B*. 2024;403:134942. doi:10.1016/j.snb.2023.134942
87. Shi X, Tian R, Wang Q, Song P. Perovskite $CsPbBr_3$ quantum dots enhanced In_2O_3 nanospheres for triethylamine detection at low temperature. *Ceram Int*. 2024;50(24, Part B):53941–53950. doi:10.1016/j.ceramint.2024.10.247